

Suppressing grid instability and noise in particle-in-cell simulation by smoothingGregory R. Werner,¹ Luke C. Adams,¹ and John R. Cary^{1,2}¹*Center for Integrated Plasma Studies, Physics Department,
University of Colorado Boulder, Boulder, CO 80309.*²*Tech-X Corp., 5621 Arapahoe Ave, Boulder, CO 80303.*(*Electronic mail: Greg.Werner@colorado.edu)

(Dated: 10 March 2025)

Smoothing short-wavelength charge density variations can stabilize explicit electrostatic particle-in-cell (PIC) plasma simulations against grid heating and cold beam instabilities, which cause unphysical heating when the Debye length is poorly resolved. We demonstrate this by solving the dispersion and by running 1D electrostatic PIC simulations, using an efficient smoothing algorithm that leverages the Poisson solve. To ensure stability, the smoothing radius must increase with the number of Debye lengths per cell. Smoothing also suppresses particle noise, which is severely exacerbated by poor resolution of the Debye length. To help determine optimal PIC configuration, we empirically characterize electric field noise, particle velocity diffusion, and unphysical energy exchanges in 1D PIC simulation, as a function of Debye-length resolution, smoothing, and particles per cell. We also show how PIC noise causes test particles to exhibit misleading behavior. Since smoothing reduces the effective resolution, the optimal cell size is less than the desired resolution but can be much greater than the Debye length, reducing computational expense.

CONTENTS

I	Introduction	2
II	Under-resolving the Debye length exacerbates PIC noise	4
III	Estimating the smoothing needed to defeat grid instability	5
IV	Smoothing with a modified Poisson solve	7
V	Grid instability growth rates for a Cauchy-squared distribution	9
VI	Results from 1D MC-PIC simulations	12
	A. MC-PIC simulation set-up	12
	B. Signatures of grid instability and noise-driven heating	13
	C. Smoothing suppresses grid instability and noise-driven heating	14
	D. Electric field noise	16
	E. Quiet and noisy starts	18
	F. Thermal energy evolution and velocity-diffusion heating	18
	G. Test particles do not always mimic MC-PIC particles	21
VII	Discussion	21
VIII	Summary	23
	Acknowledgments	26
	Author declarations	26
	Data availability	26
A	Deriving the finite difference dispersion	26
B	The dispersion integral for the Cauchy-squared distribution	29
C	The exact dispersion for a Cauchy-squared distribution	29
D	Solving the numerical dispersion for a Cauchy-squared distribution	30
	References	32

I. INTRODUCTION

Particle-in-cell (PIC) simulation has become an invaluable tool for studying plasma behavior across a wide range of fields, from beam physics to astrophysics. Its main advantage, the ability to simulate classical plasma physics from first principles, is closely related to one of its main frustrations: it can be unstable when plasma microscales (such as the electron Debye length λ_D or plasma frequency ω_p) are not resolved, even when the associated phenomena (e.g., Debye shielding, Langmuir waves) are expected to be absent in a particular application. Furthermore, PIC can be noisy, sometimes to the point of precluding feasible simulation. In this paper, we will quantify how under-resolving the Debye length introduces numerical instabilities and exacerbates noise, and we will show how both these problems can be simply and efficiently solved in standard explicit electrostatic PIC by smoothing the charge density (and we will calculate how much smoothing is needed). Thus smoothing could greatly speed computation in simulations where Debye-scale physics is unimportant. Although smoothing has been previously suggested as a way to defeat grid instability, previous works did not calculate how much smoothing is needed.

By “smoothing,” we mean filtering out short-wavelength variations in the charge density field. Its effect is similar to using larger or higher-order particle shapes (Hockney, 1971), but smoothing the field instead of individual particles is faster.

There are many variants of PIC, but the simplest explicit electrostatic and electromagnetic algorithms (especially momentum-conserving PIC with linear weighting or first-order particle shapes) continue to be widely used (Birdsall & Langdon, 2004). They are generally fastest, in terms of time steps per second, and reliably scalable, maintaining high efficiency on massively parallel supercomputers.

When explicit PIC simulations fail to resolve the Debye length, grid instability unphysically heats the plasma until the Debye length is resolved (Langdon, 1970; Okuda, 1972a,b). Grid instabilities arise when sub-grid variations in particle density alias to grid-resolved wavelengths, coupling different wavelengths that should not be physically coupled (Langdon, 1970; Birdsall & Maron, 1980). Explicit “energy-conserving” algorithms (which conserve energy precisely only in the limit of zero time step) avoid grid instability when simulating *stationary* plasma (Lewis, 1970; Langdon, 1973), and for that reason have recently received renewed attention (Barnes & Chacón, 2021; Powis & Kaganovich, 2024; Adams et al., 2025). However, they still suffer from cold beam instability, a manifestation of grid instability that heats *drifting* plasma unphysically by converting bulk kinetic to thermal energy (Okuda, 1972b; Chen et al., 1974).

Although grid instability can be disastrous for $\Delta x \gg \lambda_D$, particle noise may be the more pressing reason for using a cell size $\Delta x \lesssim \lambda_D$. For stationary plasmas, previous works have claimed a grid instability threshold around $\lambda_D/\Delta x \approx 1/\pi$ or 0.3 (Birdsall & Maron, 1980; Birdsall & Langdon, 2004), but recent studies suggest the threshold may be closer to $\lambda_D/\Delta x \approx 0.15$ (Adams et al., 2025). For $0.15 \lesssim \lambda_D/\Delta x \lesssim 1$, grid instability may be hard to detect but noise-driven (stochastic) heating can be so strong that it could be mistaken for grid instability. In principle, noise-driven heating can always be reduced by using more simulated macroparticles, but (we will show) for $\Delta x \gtrsim \lambda_D$, reducing Δx is likely a more efficient way to reduce noise. For example, a 1D simulation with $\Delta x = \lambda_D$ and 50 macroparticles per cell has the same noise level as one with $\Delta x = 2\lambda_D$ and 400 macroparticles per cell. Regardless of grid instability, $\Delta x \lesssim \lambda_D$ may be desirable because it more efficiently suppresses PIC noise.

Efforts to facilitate under-resolution of the Debye length have focused primarily on suppressing grid instability. Implicit PIC methods, with true energy conservation (for finite time step) can avoid grid instability (Chen et al., 2011; Markidis & Lapenta, 2011; Lapenta & Markidis, 2011; Chen &

Chacón, 2014). However, energy-conserving implicit methods are significantly more complicated, difficult to implement, more time-consuming per particle-step, and less well understood; explicit PIC is still much more widely used. Thus we continue to strive for explicit PIC algorithms with improved stability, especially-implemented algorithms.

Some notable explicit schemes that have been at least partially successful in suppressing grid instability in PIC (Birdsall & Maron, 1980) include displacing the grid to disrupt short-wavelength modes that have the highest unphysical growth rates (Chen et al., 1974; Brackbill & Lapenta, 1994), explicit energy-conserving PIC (cited above), high-order shape functions (Fiuza et al., 2011; Shalaby et al., 2017), reduced-order PIC that uses multiple 1D subdivisions of the primary 3D grid (Reza et al., 2022, 2023), the Particle-In-Fourier method (Evstatiev & Shadwick, 2013; Mitchell et al., 2019), and a machine-learning algorithm that takes advantage of phase-space information (Aguilar & Markidis, 2021).

Sufficient smoothing stabilizes explicit PIC, potentially offering simplicity, ease of implementation, generalizability, and performance beyond any of those methods. Suppressing grid instability with smoothing is not a new idea (Birdsall & Maron, 1980), although its effectiveness has not to our knowledge been previously demonstrated systematically or beyond incremental improvements in stability. For a particular smoothing kernel, we will calculate the smoothing radius needed to eliminate grid instability, as a function of Debye-length resolution. We will then characterize how smoothing affects grid instability growth as a function of $\lambda_D/\Delta x$ and drift velocity for uniform plasma, for standard 1D momentum-conserving PIC. Perhaps more important, we characterize electric field noise as a function of $\lambda_D/\Delta x$, the number of macroparticles per cell, and the smoothing strength, and further characterize the velocity-space diffusion caused by PIC noise, which results in an unphysical energy that grows linearly with time.

We will focus on the most common explicit, non-relativistic, momentum-conserving electrostatic PIC algorithm with linear weighting (cloud-in-cell), in 1D, applied to electron plasma with uniform immobile ion background—we will refer to this as MC-PIC when we wish to clarify that results apply to this specific algorithm. However, some results, and the general principle of smoothing, will likely apply to other explicit electrostatic PIC algorithms, and may well extend to electromagnetic PIC algorithms. In addition, smoothing may be useful for implicit algorithms that need to suppress noise when under-resolving the Debye length.

Following this introduction, §II will present a simple argument to motivate how under-resolving the Debye length can exacerbate PIC noise. For example, it will show that (for a large class of electrostatic PIC algorithms without smoothing) initializing particles with random positions will result in an unphysical (noise) electric field energy that exceeds the plasma energy when $\lambda_D \ll \Delta x$.

We will then turn to grid instability. In §III, we examine the electron-only electrostatic dispersion for finite Δx and estimate that, to eliminate grid instability with the proposed smoothing kernel, the charge density must be smoothed over a number of cells that scales as $\sim \Delta x/\lambda_D$.

In §IV we describe the smoothing used in this paper, which involves a modified Poisson solve. This method is efficient for large kernels (needed for $\lambda_D \ll \Delta x$), and is especially attractive because of its similarity to the electrostatic Poisson solve that must already be implemented in any electrostatic PIC code.

In §V we calculate grid instability growth rates by numerically solving the finite- Δx dispersion for a Cauchy-squared velocity distribution, first without and then with smoothing.

We then report on noise, grid instability, and smoothing in actual 1D MC-PIC simulations in §VI. We distinguish grid instability and noise-driven heating, and characterize the unphysical electric field fluctuations and the subsequent diffusion of particles in velocity space. We demonstrate that smoothing suppresses both grid heating and noise-driven heating, and warn against

“noisy starts” and using test particles to study particle trajectories.

Having shown how to stabilize PIC simulations for a given $\Delta x > \lambda_D$ by smoothing, we discuss how to apply this method practically, calculating the optimal cell size Δx when accounting for resolution degradation due to smoothing, and estimating potential speed-ups (§VII).

Finally, we comprehensively summarize our results in §VIII and suggest directions for future work.

II. UNDER-RESOLVING THE DEBYE LENGTH EXACERBATES PIC NOISE

PIC simulations suffer from “particle noise” due to statistical fluctuations of the macroparticles representing the particle distribution. When $\lambda_D \lesssim \Delta x$, this noise can become catastrophically disruptive. This has been noted in the development of so-called asymptotic-preserving schemes for $\lambda_D/\Delta x \rightarrow 0$, which conclude that in this limit, the Poisson equation is too sensitive to noise, and use alternative ways to find the electric field (Degond et al., 2010).

It is illuminating to estimate the electric field $E_{f\Delta x}$ resulting from charge density fluctuations over the length scale of a grid cell Δx . With ambient plasma density n , we consider density fluctuations of amplitude fn ; for completely uncorrelated particles, $f \approx M_{\text{ppc}}^{-1/2}$, where M_{ppc} is the number of macroparticles per cell. From Gauss’s law, we estimate $\nabla \cdot E_{f\Delta x} \sim E_{f\Delta x}/\Delta x \sim efn/\epsilon_0$. Writing n in terms of plasma frequency $\omega_p = \sqrt{ne^2/m\epsilon_0} = v_{\text{th}}/\lambda_D$ (assuming a somewhat thermal population of particles with temperature mv_{th}^2 and charge-to-mass ratio $\pm e/m$),

$$E_{f\Delta x} \sim f \frac{\omega_p m v_{\text{th}} \Delta x}{e \lambda_D}. \quad (1)$$

Acting on a particle over some time τ , $E_{f\Delta x}$ will cause a relative velocity change

$$\frac{\Delta v}{v_{\text{th}}} \sim \frac{e E_{f\Delta x} \tau}{m v_{\text{th}}} \sim f \frac{\Delta x}{\lambda_D} \omega_p \tau. \quad (2)$$

Therefore, under-resolving λ_D amplifies the effect of grid-scale density fluctuations, as gauged by how much $E_{f\Delta x}$ would change a particle’s velocity (relative to v_{th}) over a plasma period. Smoothing the charge density over multiple cells can reduce this noise.

This is far from the whole story; the fact that statistical fluctuations at the cell scale can generate such influential fields means that particles become strongly correlated, and in a self-consistent PIC simulation the above estimate is very wrong, as we will see in §VI (also see Touati et al., 2022; Acciarri et al., 2024a,b).

However, the above estimation applies rigorously in some situations. For example, if we initialize a plasma simulation with uniformly random particle positions, then, initially, $f \approx M_{\text{ppc}}^{-1/2}$. This statistical variation in density will result in spatial electric field fluctuations $E_{f\Delta x}$ with energy density

$$\frac{\epsilon_0}{2} E_{f\Delta x}^2 \sim M_{\text{ppc}}^{-1} \frac{nmv_{\text{th}}^2}{2} \left(\frac{\Delta x}{\lambda_D} \right)^2. \quad (3)$$

For example, initializing particles with independent random positions in a simulation with $\lambda_D = 0.1\Delta x$ and $M_{\text{ppc}} = 100$ results in an initial unphysical electric field energy rivaling the initial plasma thermal energy. Such random loading would likely invalidate the simulation, unless M_{ppc} is increased or Δx decreased. Thus non-random particle positioning becomes increasingly important

for $\lambda_D \lesssim \Delta x$. Other processes external to the fundamental PIC algorithm, such as injecting particles from boundaries or combining macroparticles, may also lead to similar statistical variation.

Fluctuations in the electric field can give (somewhat) random kicks to particles, causing stochastic diffusion in velocity space. This results in unphysical heating (as we will show in §VI) that increases strongly with $\Delta x/\lambda_D$. Importantly, noise-driven heating scales as M_{ppc}^{-1} , whereas the grid instability growth rate becomes independent of M_{ppc} in the limit of large M_{ppc} .

III. ESTIMATING THE SMOOTHING NEEDED TO DEFEAT GRID INSTABILITY

In this section, we ignore PIC noise and consider the infinite-particle limit where grid-instability theory applies. We conjecture that grid instability can be suppressed by smoothing the charge density $\rho(x)$ in a particular way that depends on $\lambda_D/\Delta x$, and using the smoothed charge density $\rho_{\text{sm}}(x)$ to calculate the electric potential ϕ . The smoothing will be described in terms of Fourier components at wavenumber k : $\tilde{\rho}_k \mapsto \tilde{\rho}_{\text{sm},k}$.

We will show that: if $\lambda_D/\Delta x > \alpha_c$ ensures stability for some α_c (which is known empirically to be of order unity), then (for $\lambda_D/\Delta x < \alpha_c$) suppressing charge density variations with $\tilde{\rho}_{\text{sm},k} = [\lambda_D/(\alpha_c \Delta x)]^2 \tilde{\rho}_k$ will stabilize a mode with wavenumber k . However: this over-stabilizes all modes except the most unstable (in particular, modes with small-enough k are already stable with $\tilde{\rho}_{\text{sm},k} = \tilde{\rho}_k$).

After that important analytical step (fully explicated below), our argument relies on more empirical grounds. First, grid instability is absent for $\alpha_c \sim 1$. Second, the most unstable mode usually has wavenumber $|k| \sim k_{\text{Nyq}} \equiv \pi/\Delta x$ (Birdsall & Maron, 1980). Third, for accuracy, long-wavelength behavior must remain (nearly) unchanged. With this in mind, we consider

$$\tilde{\rho}_{\text{sm},k} = \frac{1}{1 + k^2 r_{\text{sm}}^2} \tilde{\rho}_k \quad (4)$$

which smooths over a scale r_{sm} : variations with wavelengths much longer than r_{sm} ($k^2 r_{\text{sm}}^2 \ll 1$) are unchanged, while shorter wavelengths are smoothed out, reduced in amplitude by $\sim (kr_{\text{sm}})^{-2}$. For stability at k_{Nyq} we then need $(k_{\text{Nyq}} r_{\text{sm}})^{-2} \sim \lambda_D^2/(\alpha_c \Delta x)^2$, hence

$$\frac{r_{\text{sm}}}{\Delta x} \sim \frac{\alpha_c}{\pi} \frac{\Delta x}{\lambda_D}. \quad (5)$$

Then we hope that this smoothing profile will stabilize all other modes besides $|k| \sim k_{\text{Nyq}}$. Thus we conjecture that PIC will be stable when smoothing according to Eqs. (4) and (5).

The rest of this section presents a detailed motivation of this conjecture; while the analytical argument is illuminating, ultimately the conjecture is still a guess to be confirmed by numerical work in later sections. Readers less interested in the underlying motivation may prefer to skip to the next section.

In the following, we will examine the finite-difference plasma dispersion to show how grid instability can be suppressed by smoothing. For derivation of the dispersion and an introduction to grid instability, we refer the reader to previous works (Langdon, 1970; Birdsall & Maron, 1980; Birdsall & Langdon, 2004); however, for completeness, we derive the dispersion in Appendix A. We account for spatial discretization, but use continuous time and particle distribution (i.e., an infinite number of particles).

To find the frequencies and growth rates of electrostatic (electron-only) modes in a uniform plasma, we solve $D(k, \omega) = 0$, where the finite difference dispersion D is (cf. Appendix A of this

paper, and Sec. 8-10 of [Birdsall & Langdon, 2004](#))

$$D(k, \omega) = 1 - \frac{\omega_p^2 \kappa(k)}{K(k)^2} \sum_g \frac{|\tilde{S}_{k+k_g}|^2}{k+k_g} \int \frac{\partial_v F_0 dv}{v - \omega/(k+k_g)} \quad (6)$$

Everything to the right of ω_p^2/K^2 will be relatively unimportant for our argument, but for completeness we briefly describe the elements in the dispersion:

- Grid nodes are $x_j = j\Delta x$ for integer j .
- ω is the complex mode frequency; with time dependence $e^{-i\omega t}$, growth occurs if $\text{Im}[\omega] > 0$.
- $k \in (-\pi/\Delta x, \pi/\Delta x]$ is the (real) wavenumber.
- $k_g = 2\pi g/\Delta x$, for integer g , is the spacing between wavenumbers that alias to the same grid wavenumber. E.g., $\exp[i(k+k_g)j\Delta x] = \exp(ikj\Delta x)$ for integers j and g . The k_g are needed to describe sub-grid wavelengths of the particle distribution $f(x, v)$ and shape function $S(x)$. We sometimes write (uniquely) $q = k + k_g$, where q ranges over all real numbers.
- $\omega_p^2 = ne^2/(\epsilon_0 m)$ is the plasma frequency squared corresponding to plasma number density n .
- m is the electron mass; $-e$ is the electron charge; ϵ_0 is the vacuum permittivity.
- $f_0(x, v) = nF_0(v)$ is the initial, unperturbed velocity distribution; $F_0(v)$ is normalized to one.
- $S(j\Delta x; x) = S(j\Delta x - x)$ is the so-called shape function (cf. App. A or [Birdsall & Langdon, 2004](#)). It describes how fields are interpolated from grid node $j\Delta x$ to position x , i.e., $E(x) = \sum_j E_j S(j\Delta x - x)$, and how particle charge is deposited to the grid: a particle at x with charge q contributes to charge density $\rho_j = (q/V)S(j\Delta x - x)$ at node $j\Delta x$, where V is the volume around the node.
- $\tilde{S}_{k+k_g} = \tilde{S}_q$ is the Fourier transform of $S(x)$.
- $K(k)^2$ describes the “ ϕ -solve,” generalizing the usual Poisson solve (solving $-\nabla^2 \phi = \rho/\epsilon_0$ for ϕ) to include the effect of smoothing. In Fourier space, $K(k)^2 \tilde{\phi}_k = \tilde{\rho}_k/\epsilon_0$. The physically correct ϕ -solve has $K(k)^2 = k^2$, but with a standard 3-point finite difference Laplacian (without smoothing), $K(k)^2 = (2/\Delta x)^2 \sin^2(k\Delta x/2)$.
- $i\kappa(k)$ is the Fourier representation of the discretized gradient operator used to calculate E_j from ϕ_j . The physically correct dependence is $\kappa(k) = k$; with a standard centered finite difference (equivalent to differencing ϕ at nodes to E at edge-centers, and then interpolating E from edge-centers to nodes), $\kappa(k) = \sin(k\Delta x)/\Delta x$.

In continuous space (with translation invariance) all Fourier modes decouple, leaving only the $g = 0$ term in Eq. (6); however, the grid breaks continuous translational symmetry, coupling modes with $q = k + k_g$ for the same k but different integers g . Grid instability arises because sub-grid density variations in $f(x, v)$ (with wavenumber $k + k_g$ for $g \neq 0$) alias to or interact with electric fields with grid-resolved wavenumber k . This can lead to unphysical inverse Landau damping (i.e., growth).

Our analysis here is almost independent of the details of the dispersion and therefore applies generally to a large class of explicit electrostatic PIC algorithms; it relies on the fact that the dispersion can be written

$$D(k, \omega) = 1 - \frac{\omega_p^2}{K^2} \times \left[\begin{array}{c} \text{terms independent of } n \\ \text{and } \phi\text{-solve} \end{array} \right] \quad (7)$$

The plasma density and the ϕ -solve are completely specified by ω_p^2 and $K(k)^2$, respectively, and these appear in $D(k, \omega)$ only in the form ω_p^2/K^2 . We can exploit this to determine, for a simulation of a given plasma density, how we have to alter the ϕ -solve (K^2) to obtain stability. To do this, we

consider two simulations: one with the desired ω_p and an unknown K^2 , and another that is identical except with ω'_p such that it is stable with a ϕ -solve typically used in PIC, $K'(k)^2 \approx k^2$ [i.e., the two simulations are identical in $F_0(v)$, Δx , $S(x)$, and $\kappa(k)$, but differ in density]. If α_c is known such that PIC is stable when $\lambda'_D = \alpha_c \Delta x$, hence $\omega'_p = v_{\text{th}}/\lambda'_D = v_{\text{th}}/(\alpha_c \Delta x)$, we can stabilize the first simulation at a given k if we use a ϕ -solve such that $K(k)^2 = (\omega_p^2/\omega'^2_p)K'(k)^2 = (\alpha_c \Delta x/\lambda_D)^2 k^2$. These two simulations have the same dispersion; if one has no growing modes for a given k , the other also has no growing modes.

Altering $K(k)^2$ in this way stabilizes modes with any k , but it is overkill for all but the most unstable mode. Unfortunately, this argument does not tell us the smallest $K(k)^2/k^2$ that guarantees stability at other k . However, grid instability growth rates tend to increase as $|k|$ increases, with the fastest growth around $|k| \sim k_{\text{Nyq}} = \pi/\Delta x$ (cf. §V; also cf. [Birdsall & Maron, 1980](#)). This suggests choosing $K(k)^2/k^2$ to increase smoothly from 1 (at small k) to a maximum value $\sim (\alpha_c \Delta x/\lambda_D)^2$ at k_{Nyq} .

Thus we consider the candidate

$$K(k)^2 \sim k^2(1 + k^2 r_{\text{sm}}^2). \quad (8)$$

With r_{sm} given by Eq. (5), this ensures accuracy at long wavelengths and stability at k_{Nyq} , and we will have to verify numerically whether modes at all k are stabilized.

Equation (8) implies that the ϕ -solve is given by $k^2(1 + k^2 r_{\text{sm}}^2)\tilde{\phi}_k = \tilde{\rho}_k/\epsilon_0$. This is equivalent to Eq. (4) combined with $k^2\tilde{\phi}_k \approx \tilde{\rho}_{\text{sm},k}/\epsilon_0$. Thus this ϕ -solve has a nice physical interpretation: it yields the potential (via the usual Poisson solve) of the smoothed charge distribution $\rho_{\text{sm}}(x)$.

In summary, we estimate—and will later confirm—that smoothing the charge density ρ according to Eqs. (4) and (5) will eliminate the finite grid instability. Importantly, r_{sm} must increase as the Debye length becomes more poorly resolved. The obvious disadvantage of this approach is that it coarsens the effective resolution of the simulation from Δx to r_{sm} . We will discuss this later in §VII.

We note that the dependence $r_{\text{sm}}/\Delta x \sim \Delta x/\lambda_D$ resulted from our choice of smoothing in Eq. (4). Had we instead chosen $\tilde{\rho}_{\text{sm},k} = \tilde{\rho}_k/(1 + k^4 r_{\text{sm}}^4)$, the necessary smoothing length (to stabilize k_{Nyq}) would be $r_{\text{sm}}/\Delta x \sim (\Delta x/\lambda_D)^{1/2}$. This yields superior effective resolution, but it is less likely to stabilize modes with middling k , possibly requiring larger r_{sm} . Determining the optimal smoothing is left to future work.

In the next section, we suggest an efficient way to implement the smoothing of Eq. (4).

IV. SMOOTHING WITH A MODIFIED POISSON SOLVE

In this paper we propose that smoothing on a length scale $r_{\text{sm}} \sim \Delta x^2/\lambda_D$ can suppress grid instability and PIC noise to make simulation accurate for $\Delta x \gg \lambda_D$. For large $\Delta x/\lambda_D$, the large smoothing kernel spans many cells and may require nontrivial computation.

Smoothing can be accomplished by several means, and it is not this paper's goal to find or evaluate the best one. We merely wish to point out that a suitable smoothing operation can be performed with a modified Poisson solve. Since electrostatic PIC simulations already must perform a Poisson solve, we hope this will at most double the field solve time (however, 1D is special—see the note at the end of this section). Moreover, this method offers flexibility to handle whatever complications (e.g., variable mesh spacing) are already handled by the electrostatic solver.

Given charge density $\rho(n\Delta x)$ at grid nodes (with Fourier transform $\tilde{\rho}_k$) we wish to find the smoothed density ρ_{sm} satisfying Eq. (4) for any chosen smoothing length r_{sm} . This can be achieved

by solving

$$(-\nabla^2 + r_{\text{sm}}^{-2})\rho_{\text{sm}} = r_{\text{sm}}^{-2}\rho. \quad (9)$$

In a PIC code this can likely be solved in the same way as the Poisson solve for the potential ϕ . It may even be faster because the left-hand operator is more diagonally dominant, which reflects the fact that it has a more limited range: whereas solutions (Green functions) of $-\nabla^2\phi = \delta^3(r)$ decay in 3D as $\phi \sim 1/r$, solutions of $(-\nabla^2 + r_{\text{sm}}^{-2})\phi = \delta^3(r)$ decay as $\phi \sim e^{-r/r_{\text{sm}}}/r$.

When solving for ρ_{sm} by this method, one must consider boundary conditions. While periodic boundary conditions pose no extra difficulty (and, on a regular grid, allow simple solution via Fourier transform), other electrostatic boundary conditions may require different smoothing boundary conditions. With the modified Poisson solution, Neumann boundary conditions, $\hat{\mathbf{n}} \cdot \nabla \rho_{\text{sm}} = 0$, may seem appropriate because they conserve charge over the volume V , since (here, $\hat{\mathbf{n}}$ is the boundary surface normal)

$$\int_V (\rho_{\text{sm}} - \rho) dV = \int_V [\rho_{\text{sm}} - r_{\text{sm}}^2 (-\nabla^2 + r_{\text{sm}}^{-2}) \rho_{\text{sm}}] dV = \oint_{\partial V} r_{\text{sm}}^2 \nabla \rho_{\text{sm}} \cdot \hat{\mathbf{n}} dA \quad (10)$$

where the last integral is over the boundary surface of V .

However, other boundary conditions (such as $\rho_{\text{sm}} = 0$) may be preferable. Real boundaries tend to affect the plasma significantly, e.g., forming sheaths on the Debye scale. The choice to simulate with $\Delta x \gg \lambda_D$ may well preclude accurate boundary treatment, and compared with that neglect, the choice of smoothing boundary condition may be unimportant.

This consideration highlights another potential benefit of this method: accurate boundary treatment with variable mesh, with $\Delta x < \lambda_D$ near the boundary and $\Delta x \gg \lambda_D$ in the interior. The modification of the (negative) Laplacian matrix needed to apply smoothing simply adds r_{sm}^{-2} to the diagonal elements; it is trivial to allow $r_{\text{sm}} = r_{\text{sm}}(x)$ to vary in space without destroying important matrix properties like symmetry. If $r_{\text{sm}} \rightarrow 0$ at the boundary, the proper boundary condition is $\rho_{\text{sm}} = \rho$.

Varying the smoothing length $r_{\text{sm}}(x)$ in space could also be used to handle plasma with varying density as well as simulations with varying cell size.

Since the concept of a screened (Yukawa) potential is familiar to many, we point out that the smoothed potential ϕ is the difference between the raw potential ϕ_r , satisfying $-\nabla^2\phi_r = \rho/\epsilon_0$ and the screened potential ϕ_{scr} , $(-\nabla^2 + r_{\text{sm}}^{-2})\phi_{\text{scr}} = \rho/\epsilon_0$: $\phi = \phi_r - \phi_{\text{scr}}$.

Last, we note that in 1D (but hopefully not in 2D or 3D), the increased diagonal dominance of the modified Poisson solve can hurt performance, because (at least for uniform grids) in 1D, direct integration is likely the fastest way to solve the Poisson equation. This is essentially 2-term recursion with an initial guess for the electric field, which can be corrected afterwards to yield the overall potential gain. The recursion relation is $\phi_{j+1} = 2\phi_j - \phi_{j-1} - \rho_j \Delta x^2 / \epsilon_0$. With smoothing, however, it becomes $\phi_{j+1} = (2 + \Delta x^2 / r_{\text{sm}}^2) \phi_j - \phi_{j-1} - \rho_j \Delta x^2 / \epsilon_0$, which is unstable (Press et al., 2002); therefore, in 1D the smoothing cannot necessarily be done in the same way as the (unmodified) Poisson solve. On the other hand, if fast Fourier transforms are used for the Poisson solve, then smoothing can be accomplished with almost no extra cost. In 2D and 3D, where solution by direct integration is not possible, the Poisson solve requires more complicated matrix solves, and increased diagonal dominance may improve their performance.

We will demonstrate in the next two sections that this modified Poisson smoothing can be used effectively to eliminate grid instability at all wavelengths.

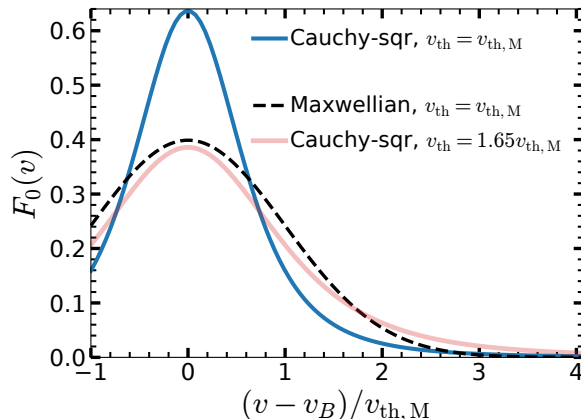


FIG. 1. A Cauchy-squared distribution $F_0(v)$ (blue line) with drift (beam) speed v_B and the same thermal speed $v_{\text{th}} \equiv \sqrt{\langle (v - v_B)^2 \rangle} = v_{\text{th},M}$ as a Maxwellian (dashed), and a Cauchy-squared distribution with $v_{\text{th}} = 1.65v_{\text{th},M}$ (pink), which has the same maximum slope as the Maxwellian.

V. GRID INSTABILITY GROWTH RATES FOR A CAUCHY-SQUARED DISTRIBUTION

In this section we calculate the growth/decay rates (and oscillation frequencies) of MC-PIC modes, in the limit of zero time step and infinitely many macroparticles (but finite Δx), by solving the numerical dispersion $D(k, \omega) = 0$ from Eq. (6), for the specific case of a Cauchy-squared distribution:

$$F_0(v) = \frac{2v_{\text{th}}^3}{\pi[v_{\text{th}}^2 + (v - v_B)^2]^2} \quad (11)$$

$$\int F_0(v) dv = 1 \quad (12)$$

$$\int v F_0(v) dv = v_B \quad (13)$$

$$\int (v - v_B)^2 F_0(v) dv = v_{\text{th}}^2 \quad (14)$$

where the drift/beam velocity v_B and the thermal velocity v_{th} are given in terms of the first and second moments. This distribution roughly resembles a Maxwellian (see Fig. 1), but simplifies numerical calculation of the dispersion roots; for reference the exact ($\Delta x \rightarrow 0$) dispersion for the Cauchy-squared distribution is solved in Appendix C. (A Cauchy distribution, $F_0(v) \propto 1/[v_{\text{th}}^2 + (v - v_B)^2]$, leads to an even simpler dispersion, but its velocity moments are inconveniently infinite.) For simplicity, we will carry on as if $F_0(v)$ were interchangeable with a Maxwellian with the same drift and thermal speeds, hence we define $\lambda_D \equiv v_{\text{th}}/\omega_p$, a choice that yields that same Bohm-Gross correction to the plasma frequency as for a Maxwellian with the same v_{th} (Appendix C). However, as Fig. 1 shows, a Cauchy-squared distribution more strongly resembles a Maxwellian for $|v - v_B| \lesssim v_{\text{th}}$ when its thermal speed v_{th} is 50%–65% higher than the Maxwellian's.

Therefore, when attempting to compare behavior with a Maxwellian, v_{th} might need to be adjusted, probably by less than a factor of 2. This uncertainty should be of little practical concern, since most PIC simulations probably cannot be trusted to contain a single perfect Maxwellian anyway.

With the Cauchy-squared distribution, we can approximate the numerical dispersion as a finite-order polynomial with analytically-determined error bounds over any given disk in the complex ω plane. The error can be made arbitrarily small by increasing the polynomial degree or decreasing the disk radius. By using many overlapping disks, each with its own polynomial approximation of $D(k, \omega)$ for which roots must be found, we can cover an area sufficient to find growth rates with desired accuracy ($10^{-6}\omega_p$) for all physical modes and all growing modes. Details of this process are given in Appendix D.

Through nondimensionalization, the normalized complex mode frequencies ω/ω_p [for which $D(k, \omega) = 0$] are functions of the three dimensionless parameters $k\Delta x$, $v_B/\omega_p\Delta x$, and $v_{th}/\omega_p\Delta x = \lambda_D/\Delta x$. We explored a 3D parameter space to characterize instability, numerically calculating the dispersion over an exhaustive set of parameters:

- $k\Delta x/\pi \in \{0.00001, \pm 0.00002, \pm 0.00005, \pm 0.0001, \pm 0.0002, \pm 0.0005, \pm 0.001, \pm 0.002, \pm 0.005, \pm 0.01, \pm 0.02, \pm 0.05, \pm 0.1, \pm 0.2, \pm 0.3, \pm 0.4, \pm 0.5, \pm 0.6, \pm 0.7, \pm 0.8, \pm 0.9, \pm 0.95, \pm 0.99\}$,
- $v_B/\omega_p\Delta x \in \{0.0001, 0.0002, 0.0005, 0.001, 0.002, 0.005, 0.01, 0.02, 0.05, 0.07, 0.08, 0.1, 0.12, 0.14, 0.16, 0.18, 0.2, 0.22, 0.24, 0.26, 0.28, 0.30, 0.32, 0.34, 0.36, 0.38, 0.4, 0.5, 1\}$,
- $\lambda_D/\Delta x \in \{0.0001, 0.0005, 0.001, 0.002, 0.005, 0.01, 0.02, 0.05, 0.07, 0.08, 0.1, 0.12, 0.14, 0.16, 0.18, 0.2, 0.22, 0.24, 0.26, 0.28, 0.3, 0.32, 0.34, 0.36, 0.38, 0.4, 0.5, 0.7, 1\}$.

We explored the effect of smoothing by considering

$$K(k)^2 = K_{\text{Poisson}}(k)^2 [1 + K_{\text{Poisson}}(k)^2 r_{\text{sm}}^2] \quad (15)$$

$$\text{where } \frac{r_{\text{sm}}}{\Delta x} = \frac{\alpha \Delta x}{\pi \lambda_D}$$

for “stability factor” $\alpha = 0$ (standard MC-PIC without smoothing), as well as smoothed MC-PIC with $\alpha = 0.2, 1$, and 5 —cf. Eq. (5). We used the standard 3-point finite-difference Poisson solve, not a Fourier solve—see the definitions of K^2 and κ after Eq. (6).

By solving the numerical dispersion, we found the maximum growth rates for MC-PIC plasma modes. Figure 2 shows the maximum growth rate (over all k), normalized to the plasma frequency, as a function of $v_B/\omega_p\Delta x$ and $\lambda_D/\Delta x$. Growth rates below $10^{-6}\omega_p$ may be below the error of the calculation, and hence may be consistent with zero. With no smoothing (Fig. 2a, $\alpha = 0$, i.e., standard MC-PIC), simulations with $\lambda_D/\Delta x \gtrsim 0.14$ are stable and those with $\lambda_D/\Delta x \lesssim 0.02$ are highly unstable, regardless of v_B . For $v_B/\omega_p\Delta x \gtrsim 10^{-2}$, the transition from stability to strong instability is very rapid; for $\lambda_D/\Delta x$ just 20% below instability threshold, the growth rate is within an order of magnitude of the maximum observed growth rate of about $0.22\omega_p$.

In the limit of large v_B , the instability threshold (without smoothing) approaches a constant that can be calculated analytically, $\lambda_D/\Delta x \approx 0.092$ (which agrees with Fig. 2); in this limit we can neglect all but one term (one value of g) in the sum in Eq. (6), yielding a cubic equation that can be solved in the same way as the exact dispersion (see Appendix C). For a drifting Maxwellian plasma, Birdsall & Maron (1980) find, experimentally, that the instability threshold is $\lambda_D/\Delta x \approx 0.046$ (in the large v_B limit). We speculate that it is not $v_{\text{th}}^2 \equiv \langle (v - v_B)^2 \rangle$ that determines grid instability in this case. Instead, the maximum slope of $F_0(v)$ may be the critical factor, since it determines the Landau damping rate (for weak damping). In this case, a Cauchy-squared distribution with $v_{\text{th}} = 1.65v_{\text{th},M}$ is “equivalent” to a Maxwellian with $v_{\text{th}} = v_{\text{th},M}$ (Fig. 1). Defining $\lambda_{D,M} \equiv v_{\text{th},M}/\omega_p$, we would expect the Cauchy-squared simulation to be stable (in the large v_B limit) for $\lambda_D/\Delta x = 1.65\lambda_{D,M}/\Delta x > 0.092$, or $\lambda_{D,M}/\Delta x > 0.056$, very close to the value of 0.046.

For $v_B \rightarrow 0$ (without smoothing), we find (looking at Fig. 2, $\alpha = 0$) that the instability threshold is roughly $\lambda_D/\Delta x \approx 0.04$ for $v_B/\omega_p\Delta x \sim 10^{-4}$, but we do not know how to extrapolate this to

Smoothing away grid instability and noise in PIC

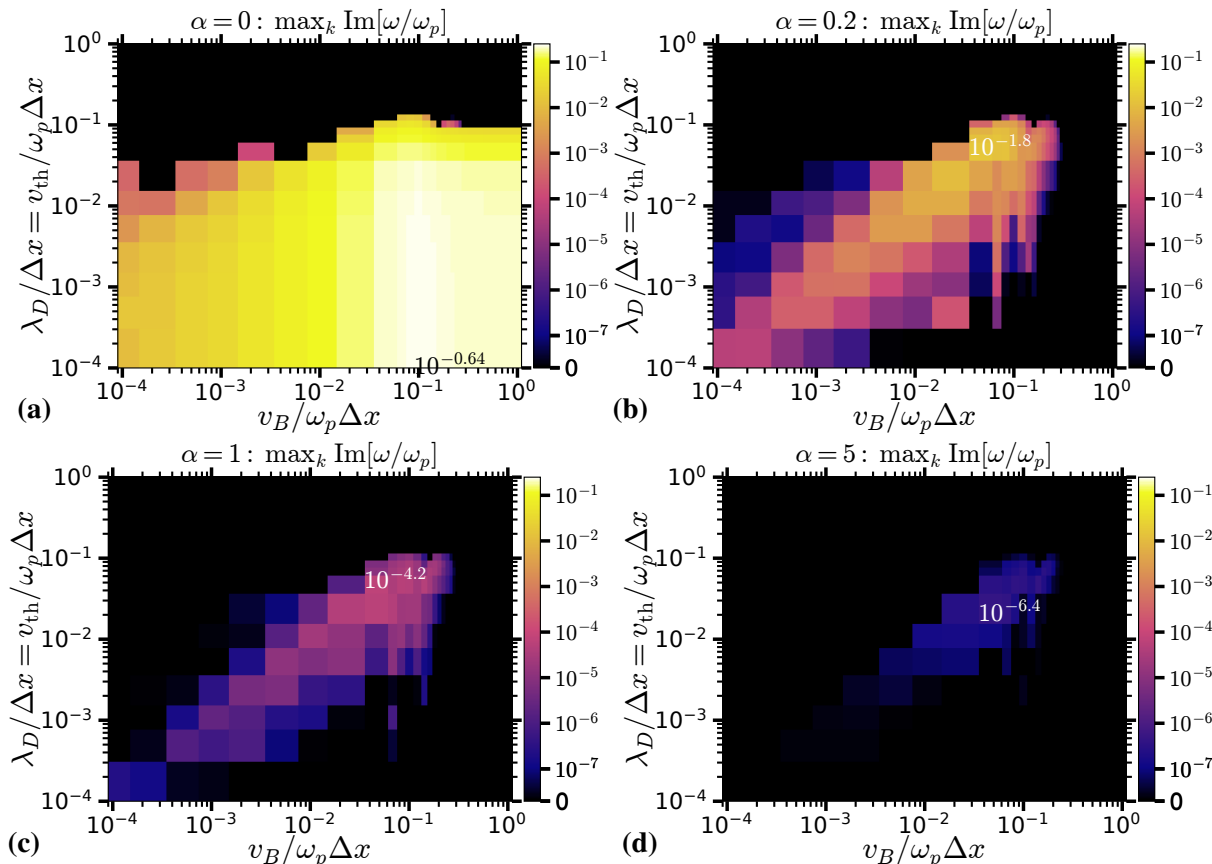


FIG. 2. Increasing the smoothing length $r_{sm} = (\alpha/\pi)\Delta x^2/\lambda_D$, for smoothing with Eq. (15), stabilizes grid heating. The panels show, for $\alpha = 0$ (standard PIC), 0.2, 1, and 5, the maximum growth rate (over all k), normalized to the plasma frequency, for MC-PIC simulation of uniform electron plasma initialized with a Cauchy-squared distribution, Eq. (11), that has normalized drift velocity $v_B/\omega_p \Delta x$ and thermal velocity $v_{th}/\omega_p \Delta x = \lambda_D/\Delta x$. The maximum value over each plot is labeled on each plot. Measurements below $10^{-6}\omega_p$ are possibly consistent with zero.

$v_B = 0$. This threshold is significantly lower than the estimate $\lambda_D/\Delta x \approx 0.15$ from running MC-PIC simulations with Maxwellian distributions (Adams et al., 2025). We do not have a good explanation for this difference. In any case, the exact threshold value is only of theoretical interest, except possibly for simulations with extremely high M_{ppc} ; most simulations will be ruined by particle noise if they run anywhere near the grid instability threshold.

Increasing the smoothing to $\alpha = 0.2$ (Fig. 2b), i.e., smoothing over $r_{sm}/\Delta x = 0.06\Delta x/\lambda_D$ cells, significantly reduces instability growth rates, stabilizing simulations with $v_B/\omega_p \Delta x > 0.3$, but the maximum growth rate of $0.016\omega_p$ is likely still too high for most simulations. A further increase to $\alpha = 1$ (Fig. 2c), or $r_{sm}/\Delta x = 0.3\Delta x/\lambda_D$, reduces the growth rates by another 2 orders (maximum: $6 \times 10^{-5}\omega_p$). Using $\alpha = 2$ (not shown, $r_{sm}/\Delta x = 0.6\Delta x/\lambda_D$) reduces the maximum growth rate to $6 \times 10^{-6}\omega_p$, and $\alpha = 5$ (Fig. 2d, $r_{sm}/\Delta x = 1.6\Delta x/\lambda_D$) reduces it below $10^{-6}\omega_p$ (we measure $4 \times 10^{-7}\omega_p$; however, since our numerical calculation may have errors as high as $10^{-6}\omega_p$, this may be consistent with zero).

Thus smoothing suppresses grid instability. Our prediction in §III was that if $\lambda_D/\Delta x \gtrsim \alpha_c \approx 0.14$ ensures stability without smoothing, as Fig. 2(a) suggests, then smoothing with $\alpha = \alpha_c = 0.14$

would marginally stabilize the Nyquist mode, $k\Delta x = \pi$. This appears to be the case, but stabilizing $k = \pi/\Delta x$ is not sufficient: modes with smaller k must also be stabilized, and the smoothing affects them less than the Nyquist mode.

As we increase the smoothing length r_{sm} , the fastest growing modes shift to smaller k . Almost all the fastest growing modes for $\alpha = 0$ (no smoothing, standard MC-PIC) have $|k_{\text{fastest}}|\Delta x > 0.7\pi$ (for comparison, using a Fourier Poisson-solve results in the fastest modes having $|k_{\text{fastest}}|\Delta x \approx \pi$; when we use the 3-point finite-difference Poisson solve, the subsequent interpolation of edge E to nodal E yields $\kappa(\pi/\Delta x) = 0$, eliminating the Nyquist mode). For $\alpha = 0.2$, $|k_{\text{fastest}}|\Delta x < 0.6\pi$; for $\alpha = 1$, $|k_{\text{fastest}}|\Delta x < 0.1\pi$, and for $\alpha = 5$, $|k_{\text{fastest}}|\Delta x < 0.02\pi$. (In this last case, our coverage of k becomes pretty sparse around k_{fastest} , so we could potentially miss some more unstable modes; however, MC-PIC simulation in the following section backs up these results.) We speculate that for $\alpha \lesssim 0.14$, $|k_{\text{fastest}}|\Delta x \sim \pi$ and for $\alpha \gtrsim 0.14$, $|k_{\text{fastest}}|\Delta x \sim 0.14\pi/\alpha$. In achieving stability, our smoothing [i.e., a low-pass filter of ρ with Fourier profile $(1 + k^2 r_{\text{sm}}^2)^{-1}$] overstabilizes the shortest-wavelength modes. There may be more optimal filters that achieve stability with less degradation of the spatial resolution; we leave such questions to future work.

We have thus shown how smoothing suppresses grid instabilities for a Cauchy-squared distribution. We have also characterized grid instability growth rates, as a function of $v_B/\omega_p\Delta x$ and $\lambda_D/\Delta x$, for standard MC-PIC (with a Cauchy-squared distribution) without smoothing. Although grid instability is absent for $\lambda_D/\Delta x \gtrsim 0.14$ (for any v_B), under-resolving the Debye length (without smoothing) can still lead to problems with particle noise, which is absent in the preceding treatment, since it assumes an infinite number of particles. We will investigate the effect of smoothing on grid instability and PIC noise using full 1D MC-PIC simulation in the following section.

VI. RESULTS FROM 1D MC-PIC SIMULATIONS

Although solving the numerical dispersion is a powerful tool for understanding PIC simulation, it does not include the effects of finite time step or a finite number of particles. Therefore we test smoothing directly with a simple 1D MC-PIC simulation, and investigate how PIC noise depends on $\lambda_D/\Delta x$ (as well as other parameters, including M_{ppc} and r_{sm}).

A. MC-PIC simulation set-up

We implemented the standard MC-PIC algorithm: leapfrogged momentum-conserving electrostatic PIC (with linear weighting, sometimes called area weighting or cloud-in-cell; [Birdsall & Langdon, 2004](#)) with one spatial and one velocity dimension, using a 3-point finite-difference Poisson solve, coded in Python. We used a regular grid with N cells and cell size Δx , hence length $L = N\Delta x$, and periodic boundary conditions.

We initialized electrons with M_{ppc} macroparticles per cell, evenly distributed to yield zero initial electric field (except in §[VIE](#), where we explore random initial positions, leading to non-zero random initial electric field). The field solve assumed a uniform compensating positive charge. Each electron was given a velocity drawn from a random 1D Maxwellian distribution (not a Cauchy-squared distribution as used above) with drift velocity v_B and thermal velocity v_{th} . We note that the actual average velocity differs from v_B by order $v_{\text{th}}/\sqrt{NM_{\text{ppc}}}$ due to statistical variation. (However, in §[VIE](#), we explore “quiet” starts with particles initially ordered in phase space.)

We applied smoothing (at each time step) with strength α as described in §[IV](#); i.e., the smoothing radius is $r_{\text{sm}}/\Delta x = (\alpha/\pi)\Delta x/\lambda_D$ cells.

Smoothing away grid instability and noise in PIC

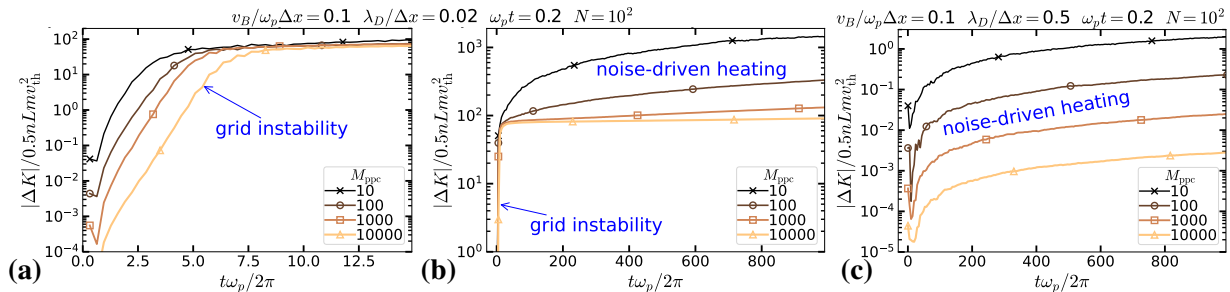


FIG. 3. Grid instability and noise-driven heating have different M_{ppc} -dependence. Each panel shows the magnitude of plasma kinetic energy change over time, normalized to the initial thermal energy, for MC-PIC simulations with no smoothing ($\alpha = 0$) and M_{ppc} ranging from 10 to 10^4 . Panels (a) and (b) show the same simulation with $\lambda_D/\Delta x = 0.02$ (and $v_B/\omega_p\Delta x = 0.1$). (a) In the first few plasma periods, grid instability causes exponential energy growth; the effect of M_{ppc} on the growth rate and saturation energy diminishes for large M_{ppc} . (b) Over longer times, particle noise causes additional unphysical heating. (c) A simulation with $\lambda_D/\Delta x = 0.5$ (and $v_B/\omega_p\Delta x = 0.1$) exhibits no grid instability, but does suffer from noise-driven heating, which scales as M_{ppc}^{-1} .

We varied the time step Δt from simulation to simulation, always keeping it below the maximum stable value. Given a maximum plasma mode frequency ω_{max} , the leapfrog time advance requires $\omega_{\text{max}}\Delta t < 2$ for stability (although $\omega_{\text{max}}\Delta t \ll 1$ is required for accuracy at frequency ω_{max}). Often the highest frequency is simply ω_p ; however, with a drifting plasma, $\omega = kv_B \pm \omega_p$, possibly requiring a smaller time step. In addition, it is important for stability and accuracy that most particles travel less than Δx in one time step (Brackbill & Forslund, 1982). Since $v_{\text{th}} = \lambda_D\omega_p$, the stability criterion $(\pi v_B/\Delta x + \omega_p)\Delta t < 2$ means that $v_{\text{th}}\Delta t/\Delta x < 2/(\pi v_B/v_{\text{th}} + \Delta x/\lambda_D)$ and so whenever $\lambda_D/\Delta x \ll 1$, the cell-crossing criterion is always met; for $\lambda_D/\Delta x \gtrsim 1$, we have to reduce the time step. We ran simulations for a time T , which we will usually express in terms of the plasma period $2\pi/\omega_p$; we ran some simulations up to $T = 2\pi 10^4/\omega_p$.

We carried out all simulations with $\lambda_D = 1$ m, $\omega_p = 1$ s, hence $v_{\text{th}} = 1$ m/s, and varied Δx , L , v_B , M_{ppc} , r_{sm} , and Δt . Thus we explored stability and noise over the 6-dimensional parameter space of dimensionless parameters $v_B/\omega_p\Delta x$, $\lambda_D/\Delta x = v_{\text{th}}/\omega_p\Delta x$, M_{ppc} , $\alpha = r_{\text{sm}}/\Delta x$, $\omega_p\Delta t$, and $N = L/\Delta x$. Our results scale trivially to any choice of λ_D and ω_p .

When we discuss results below, we will specify the values of these parameters. We will hardly mention the effect of N , which is negligible as long as $N \gg 1$ and $r_{\text{sm}}/\Delta x \ll N$. Similarly, decreasing the time step had negligible effect on the results reported here.

B. Signatures of grid instability and noise-driven heating

We start by showing MC-PIC simulation without smoothing. Figure 3 shows the time evolution of (the absolute value of) the net change in kinetic energy $\Delta K(t)$ for two cases, one with $\lambda_D/\Delta x = 0.02$ that suffers grid instability and one with $\lambda_D/\Delta x = 0.5$ that does not. Both cases have $v_B/\omega_p\Delta x = 0.1$, $N = 100$ cells, and time step $\omega_p\Delta t = 0.2$; in each case, we show four simulations with different M_{ppc} . In the first few plasma periods of the unstable case (Fig. 3a) $\Delta K(t)$ grows exponentially; the electric field energy grows at about the same rate (not shown). As M_{ppc} increases, the exponential growth in energy ($\sim e^{2\gamma t}$) appears to converge to rate $\gamma \approx 0.2\omega_p$, roughly as we calculated in Fig. 2 (for a slightly different velocity distribution F_0). This exponential growth sat-

urates at a level nearly independent of M_{ppc} , about 60 times the initial plasma energy (while the electric field energy grows to about 10 times the initial plasma energy). Increasing the energy by 60 times increases $\lambda_D/\Delta x$ to about $0.02\sqrt{60} \approx 0.15$, which is roughly where we expect stability (albeit for a Cauchy-squared distribution, Fig. 2; this agreement is probably coincidentally closer than the uncertainties of this estimate).

However, over longer times (Fig. 3b, showing $|\Delta K(t)|$ for the same simulation out to 1000 plasma periods) the energy continues to grow unphysically at a rate that depends strongly on M_{ppc} . With $M_{\text{ppc}} = 10^4$, the additional heating over 1000 plasma periods is noticeable but small compared with the grid instability heating. For $M_{\text{ppc}} = 10$, however, the noise-driven heating increases the energy by another order of magnitude.

In Fig. 3(c), we show $|\Delta K|$ over time in a marginally-resolved case with $\lambda_D/\Delta x = 0.5$, again for different M_{ppc} . Immediately after initialization, the electrons lose some energy to the electric field, which is initially zero (cf. §VIF); thus ΔK is negative at very early times, and then grows, rising through zero and becoming large and positive. None of these simulations show an exponential growth phase; grid instability is absent. Nevertheless, the energy grows unphysically due to stochastic noise-driven heating. The growth is strongly M_{ppc} -dependent: $\Delta K(t) \propto M_{\text{ppc}}^{-1}$. For $M_{\text{ppc}} = 10$ heating is significant after just a few tens of plasma periods, but for $M_{\text{ppc}} = 1000$, ΔK grows to only a couple percent of the initial kinetic energy over 1000 periods. The energy grows roughly linearly in time, consistent with particles exhibiting a random walk in velocity space.

Thus we distinguish grid instability heating from noise-driven (stochastic) heating. Grid instability causes exponential growth independent of M_{ppc} for sufficiently large M_{ppc} . It saturates when the Debye length increases to $\lambda_D/\Delta x \sim 0.1$. However, with $\lambda_D/\Delta x \lesssim 1$, particle noise is enhanced (cf. §II). Field fluctuations due to statistical particle noise (cf. §VID) cause diffusion in velocity space, leading to unphysical heating that scales as M_{ppc}^{-1} (and grows linearly in time; cf. §VIF).

C. Smoothing suppresses grid instability and noise-driven heating

We now demonstrate that smoothing can eliminate grid instability in actual PIC simulation, confirming the results of §V (but for Maxwellian distributions); we will also see that smoothing suppresses noise-driven heating. Figure 4 shows the kinetic energy versus time for four very under-resolved cases [with $(v_B/\omega_p\Delta x, \lambda_D/\Delta x)$ equal to $(0, 0.005)$, $(0.02, 0.01)$, $(0.1, 0.02)$, and $(0.002, 0.0005)$]. In each case, we show the simulations with different smoothing lengths, $\alpha = 0.2, 0.5, 1, 2$, and 5 (also labeling the smoothing radius in cells, $r_{\text{sm}}/\Delta x$). They all run for 10^4 plasma periods. Three have $N = 10^4$ and $M_{\text{ppc}} = 10$, and the one with worst Debye resolution has $N = 10^5$ (so that $r_{\text{sm}} \ll L$) and $M_{\text{ppc}} = 1$. The time step, $\omega_p\Delta t = 1.8$, is large—too large for accurate measurement of plasma frequencies, but it shows that, despite v_B , one can use a time step nearly up to $\omega_p\Delta t = 2$. A smaller time step yields similar stability and should render Langmuir waves accurately if their wavelength is long compared to r_{sm} .

All these simulations are highly unstable for $\alpha = 0$ (not shown), with unphysical energy gains of multiple orders of magnitude over tens of plasma periods. A little smoothing ($\alpha = 0.2$) reduces unphysical heating substantially, taking thousands of plasma periods to increase the energy by a disastrous factor of 100. With $\alpha = 1$, the unphysical energy gain over 10^4 plasma periods is of the order of the initial energy (or several times that, when $M_{\text{ppc}} = 1$). With $\alpha = 2$, however, simulation is reasonable, at least for short times (hundreds or thousands of plasma periods), and $\alpha = 5$ is sufficient to avoid unphysical heating for 10^4 plasma periods. With $\alpha = 5$, the particle distribution after 10^4 plasma periods looks essentially identical to the initial distribution (with 10^6 particles in the simulation, the distributions can be compared out to velocities about $3.9v_{\text{th}}$ from

Smoothing away grid instability and noise in PIC

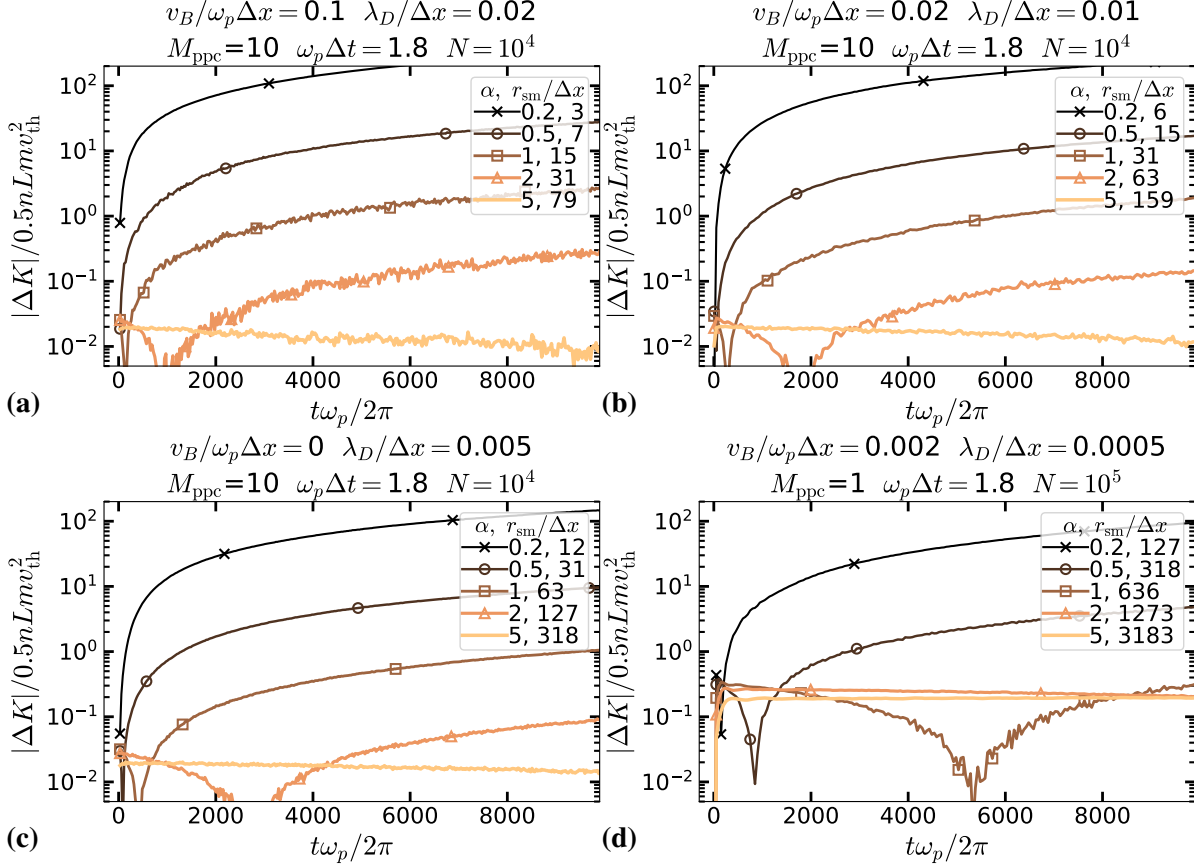


FIG. 4. Smoothing suppresses grid instability (which is so strong without smoothing that it would just be a spike on the left side of these graphs) and noise-driven heating. These plots show the magnitude of plasma kinetic energy change $|\Delta K|$ over 10^4 plasma periods, for four 1D MC-PIC simulations with different $v_B/\omega_p\Delta x$ and $\lambda_D/\Delta x$ (labeled at the top of each panel, along with M_{ppc} , the time step, and number of cells), each with different amounts of smoothing: $\alpha = 0.2, 0.5, 1, 2,$ and 5 (the corresponding $r_{\text{sm}}/\Delta x$ is labeled for each α). While $\alpha = 1$ might be tolerable (especially for shorter times), $\alpha = 5$ provides robust simulation for long times. In the severely under-resolved case with $\lambda_D/\Delta x = 0.0005$ (panel d), only $M_{\text{ppc}} = 1$ is used, and the resulting noise causes $|\Delta K|$ to be immediately $\sim 20\%$ of the initial energy for $\alpha \gtrsim 1$; this can be reduced to about 2% by using $M_{\text{ppc}} = 10$ (as seen in the other panels).

the mean); for the $(0.02, 0.01)$ case, we measured the same $v_B/\omega_p\Delta x$ to high precision (because the algorithm is momentum conserving), while $v_{\text{th}}/\omega_p\Delta x$ changed by -0.6% .

Even for $\alpha = 0.2$, the energy growth, hence the need for large r_{sm} , appears to be driven primarily by noise, not grid instability (cf. Fig. 3). Interestingly, with sufficient smoothing, the noise level no longer depends on r_{sm} ; this is especially clear for $M_{\text{ppc}} = 1$, where $|\Delta K|$ is roughly the same for $\alpha = 2$ and $\alpha = 5$. Moreover, for $\alpha = 5$, $|\Delta K| \approx 0.2M_{\text{ppc}}^{-1}$ for all 4 cases. (This is discussed more in §VIF.)

Smoothing also allows large time steps $\omega_p\Delta t \approx 2$, even for large drift velocities (probably because high- k modes are suppressed by smoothing). With explicit time-stepping, we cannot exceed $\omega_p\Delta t = 2$ because plasma oscillations still have frequency ω_p at the longest wavelengths (we have observed problems for $\omega_p\Delta t$ just slightly less than 2, but as we show above, $\omega_p\Delta t = 1.8$ works well).

Smoothing away grid instability and noise in PIC

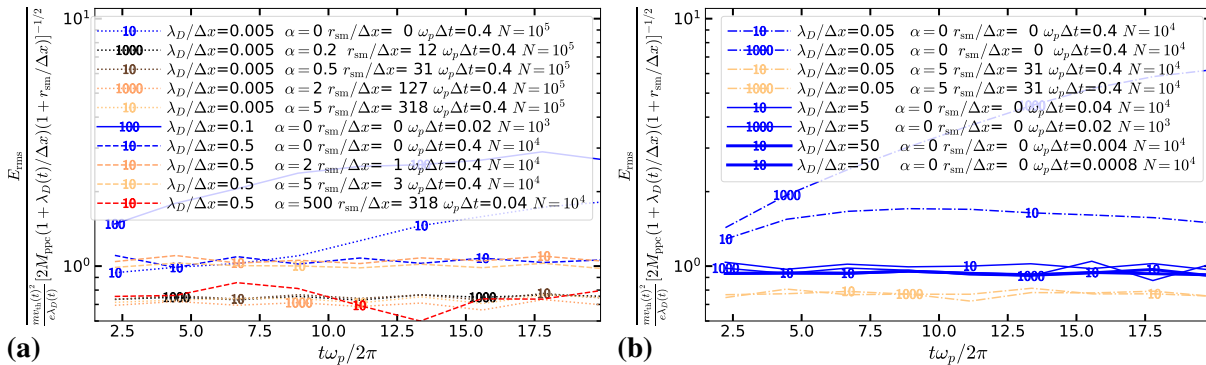


FIG. 5. The point of these plots is merely that all the values are of order one, confirming that Eq. (16) is a decent estimate of the “noise field” E_{rms} for a wide range of $\lambda_D/\Delta x$, M_{ppc} , α , $\omega_p\Delta t$, and N . The two panels both show E_{rms} normalized to Eq. (16) over 20 plasma periods for different sets of simulations with $v_B = 0$. The varied parameters are labeled in the legend, except for $M_{\text{ppc}} \in \{10, 100, 1000\}$, which is written on the curves. We make no attempt to explain the variations beyond Eq. (16). Here, the normalization depends on time through $v_{\text{th}}(t)$ and $\lambda_D(t)$, which may be significant for simulations with $\lambda_D/\Delta x \ll 1$ and no smoothing.

Because $\lambda_D/\Delta x$ is so small in these cases, smoothing with $\alpha = 5$ requires large smoothing radii r_{sm} of 80, 160, 320, and 3200 cells in the four cases shown in Fig. 4. Moreover, r_{sm} is the characteristic exponential decay length of the smoothing kernel, which thus extends somewhat beyond r_{sm} .

The stabilizing of extremely under-resolved simulations with $\lambda_D/\Delta x = 5 \times 10^{-4}$ and $M_{\text{ppc}} = 1$ dramatically confirms the effectiveness of this approach. However, smoothing over even $r_{\text{sm}}/\Delta x = 80$ cells seems repugnant at first because it significantly degrades the spatial resolution; nevertheless, as we will discuss in §VII, this would be done in a situation where the desired resolution is $\Delta x_{\text{ideal}} \sim 80^2 \lambda_D$, and such smoothing enables the use of $\Delta x \sim 80 \lambda_D$, a cell size 80 times larger than unsmoothed MC-PIC could use, likely speeding up simulation by more than a factor of 80.

D. Electric field noise

It is particularly important to understand the effects of noise when under-resolving the Debye length. In this section we characterize the electric field noise in MC-PIC simulations with and without smoothing. For brevity, we focus mostly on cases with zero drift velocity, $v_B = 0$.

When each macroparticle represents many electrons, randomness in macroparticle positions can lead to unphysical electric field fluctuations. After initializing a simulation with evenly-spaced (perfectly correlated) macroparticles yielding $E = 0$, the root mean square electric field variation, E_{rms} , increases over time but remains much less than $E_{f\Delta x}$ in Eq. (1) with $f \sim M_{\text{ppc}}^{-1/2}$, which applies to completely uncorrelated particle positions. Thus particles become less correlated but far from uncorrelated.

We find empirically (at least for $v_B = 0$) that the root-mean-square electric field is

$$E_{\text{rms}} \sim \frac{mv_{\text{th}}^2}{e\lambda_D} \frac{1}{\sqrt{2M_{\text{ppc}}(1 + \lambda_D/\Delta x)(1 + r_{\text{sm}}/\Delta x)}} \quad (16)$$

where v_{th} and λ_D are immediate values (not initial values). This is demonstrated in Fig. 5, which shows E_{rms} calculated over the whole simulation length at regular times over the first 20 plasma

Smoothing away grid instability and noise in PIC

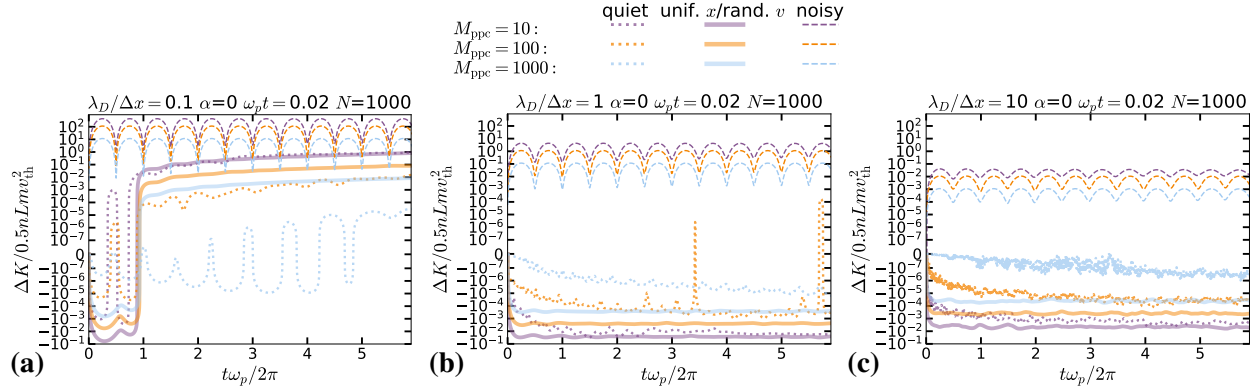


FIG. 6. The (unphysical) change ΔK in total particle energy over six plasma periods, for different particle initialization strategies, shown for $\lambda_D/\Delta x = 0.1, 1,$ and 10 (left to right), and for different $M_{\text{ppc}} \in \{10, 100, 1000\}$ (purple, orange, light blue). Dotted lines show a quiet start with ordered positions and velocities, yielding the smallest $|\Delta K|$ for given $\lambda_D/\Delta x$ and M_{ppc} . Thick, solid lines show ordered positions with random velocities (used throughout this paper)—this does nearly as well as a quiet start for small M_{ppc} . Thin, dashed lines show a noisy start with random positions and velocities; the random positions immediately create a large electric field (cf. §II) that sloshes to the particles at the plasma frequency. When starting with ordered positions, hence $E = 0$, particles initially lose energy to the electric field; a quiet start (at least with $\lambda_D/\Delta x \gtrsim 1$) prolongs this phase. For $\lambda_D/\Delta x = 0.1$, noise-driven heating starts after just one plasma period for ordered positions with random velocities; a quiet start can delay this too, and reduce noise-driven heating, although eventually (even in this uniform plasma) its initial correlations will be lost. All simulations have $v_B = 0$, $\omega_p t = 0.02$, and no smoothing.

periods, for $v_B = 0$. The measured values of E_{rms} over this time are almost all within a factor of 2 of Eq. (16), for parameters ranging in $0.005 \leq \lambda_D/\Delta x \leq 50$, $10 \leq M_{\text{ppc}} \leq 10^3$, $0.0008 \leq \omega_p \Delta t \leq 0.4$, $0 \leq \alpha \leq 5$, $10^4 \leq N \leq 10^5$. In 2 cases ($\lambda_D/\Delta x = 0.05$, $\alpha = 0$ and 0.2), E_{rms} evolved over time to be about 2.5 times and about 6 times higher than Eq. 16 after 20 plasma periods. Unlike $E_{f\Delta x}$ in Eq. (16), the self-consistent E_{rms} depends only weakly on $\lambda_D/\Delta x$ for $\lambda_D < \Delta x$.

In terms of energy density (making use of $v_{\text{th}} = \lambda_D \omega_p$),

$$\frac{\epsilon_0}{2} E_{\text{rms}}^2 \sim \frac{nmv_{\text{th}}^2}{4M_{\text{ppc}}(1 + \lambda_D/\Delta x)(1 + r_{\text{sm}}/\Delta x)} \quad (17)$$

suggesting that simulations with $\lambda_D \lesssim \Delta x$ and $r_{\text{sm}} = 0$ are near *numerical* equipartition with the field energy per cell equal to the thermal energy of one macroparticle, $(\epsilon_0/2)E^2 = nmv_{\text{th}}^2/(2M_{\text{ppc}})$ (we speculate that the factor of 2 discrepancy here might be related to the particle shape spanning two cells, which provides a small amount of smoothing even when $r_{\text{sm}} = 0$; Hockney, 1971). This agrees well with analytical predictions of Touati et al. (2022) for 1D PIC with no smoothing, $(\epsilon_0/2)E_{\text{rms}}^2 \sim (1/4)(nmv_{\text{th}}^2/M_{\text{ppc}})(2\Delta x/\pi\lambda_D) \tan^{-1}(\pi\lambda_D/2\Delta x)$. I.e., $\tan^{-1}(x)/x \approx (1 + 2x/\pi)^{-1}$ within 25% error, which is less than the scatter of our measurements. Smoothing or resolving λ_D decreases E_{rms} below numerical equipartition with macroparticles.

E. Quiet and noisy starts

Since a uniform plasma (with an infinite number of particles) would have $E = 0$, E_{rms} is the “noise” field that depends on how interactions between particles correlate their positions. Anything that places particles in positions via mechanisms other than the PIC algorithm may yield different noise levels. For example, initializing a simulation by placing particles at *random* positions will yield $E_{\text{rms}} \sim E_{f\Delta x}$ with $f \approx M_{\text{ppc}}^{-1/2}$ from Eq. (1).

Figure 6 shows the change in plasma energy ΔK over the first six plasma periods, for three different initialization strategies, for $\lambda_D/\Delta x \in \{0.1, 1, 10\}$ and $M_{\text{ppc}} \in \{10, 100, 1000\}$. A “noisy” start (dashed lines), with *random* initial positions and velocities, immediately introduces a relatively large unphysical electric field $\sim E_{f\Delta x}$ (also see Acciarri et al., 2024a,b); the field energy is transferred to particles via conspicuous plasma oscillations. For $\lambda_D/\Delta x = 0.1$ (Fig. 6a), even $M_{\text{ppc}} = 10^3$ introduces an unphysical energy ten times the initial plasma energy. For $\lambda_D/\Delta x = 1$ (Fig. 6b), $M_{\text{ppc}} = 10^2$ still yields 100% unphysical energy gain (this falls to 10% for $M_{\text{ppc}} = 10^3$). In contrast, for $\lambda_D/\Delta x = 10$ (Fig. 6c), a noisy start with $M_{\text{ppc}} > 10$ yields an initial field energy less than a few percent of the plasma energy.

The thick lines show the result of initially *uniformly-spaced* positions with *random* velocities (like most simulations in this paper). Here, ΔK is negative at early times, because the electric field is initially zero and immediately gains some energy from particles (this is discussed more in §VIF).

For comparison, we also show a “quiet” start (dotted lines), initialized with equal-weight particles “*evenly*” spaced in both position and velocity (Byers & Grewal, 1970; Birdsall & Langdon, 2004). The generated velocities were spaced within intervals along the velocity axis such that every interval had the same area under the velocity distribution $f(v)$. (In the same equal-area sense, each velocity was located at the “middle” of its interval.) The velocities, at first ordered monotonically, were then scrambled via a bit-reversal permutation. Even quieter starts are possible, in particular using ordered velocities in one cell and copying the particles exactly into the other cells, but such high order can introduce new instabilities (Gitomer & Adam, 1976). In any case, the low-noise correlations will be lost over time, especially with small M_{ppc} . For small $M_{\text{ppc}} \sim 10$, the difference between random and ordered velocities can be pretty insignificant. Even for $M_{\text{ppc}} = 100$, after only 20 plasma periods (not shown) the unphysical energy with a quiet start is just a factor of 3 lower than with uniform positions and random velocities.

Incidentally, grid instability occurs for $\lambda_D/\Delta x = 0.1$ in Figure 6(a), but it is essentially undetectable because it is swamped by noise-driven heating, even for $M_{\text{ppc}} = 1000$ with a quiet start. Using much higher M_{ppc} would reveal the exponential energy growth due to grid instability.

F. Thermal energy evolution and velocity-diffusion heating

In our MC-PIC simulations of uniform plasma that do not exhibit grid instability (with initially evenly-spaced positions and random velocities), we observe the following evolution of the plasma thermal energy, which should ideally remain constant: (we note that with momentum-conserving PIC, the bulk drift energy does remain constant)

- Initially, the plasma has thermal energy density $U_i = nmv_{\text{th},i}^2/2$.
- Stage 1. Almost immediately (in less than a plasma period) the plasma loses energy density $\epsilon_0 E_{\text{rms}}^2/2$ [cf. Eq. (17)] to the electric field, roughly conserving energy overall. For $\lambda_D \lesssim \Delta x$ and $r_{\text{sm}} = 0$, the plasma and field thus reach numerical equipartition immediately.

Smoothing away grid instability and noise in PIC

- Stage 2 (applicable only for $r_{\text{sm}} > \Delta x$). Over time $t_{\text{decl}} \sim (1 + r_{\text{sm}}/\Delta x)/(\sqrt{2}\omega_p)$, the thermal energy density declines further, linearly in time, until it reaches $U_{\text{min}} \sim U_i(1 - 0.3/M_{\text{ppc}})$. If the electric field gained this energy, the system would near numerical equipartition; that does not happen, however, and this change violates energy conservation. With strong smoothing, we have observed U_{min} closer to $U_i(1 - 0.2/M_{\text{ppc}})$; unfortunately, smoothing has little effect on U_{min} , although it does lengthen t_{decl} .
- Stage 3 (noise-driven heating). The thermal energy density grows linearly in time due to stochastic velocity diffusion (for which we find an empirical formula below). The electric field energy also grows correspondingly, violating energy conservation.

(N.B. We have not investigated the regime where both $\lambda_D > \Delta x$ and $r_{\text{sm}} > 0$.) We find empirically that the rate of change of the plasma thermal energy K_{th} is given in these three stages roughly by

$$\frac{1}{\omega_p K_{\text{th}}(t)} \frac{dK_{\text{th}}}{dt}(t) \sim \begin{cases} -\frac{\delta(\omega_p t)}{2M_{\text{ppc}}(1+\lambda_D/\Delta x)(1+r_{\text{sm}}/\Delta x)} & \text{for } \omega_p t \approx 0 \\ -\frac{0.3\sqrt{2}}{M_{\text{ppc}}(1+r_{\text{sm}}/\Delta x)} & \text{for } 0 \lesssim \omega_p t \lesssim \frac{1+r_{\text{sm}}/\Delta x}{\sqrt{2}} \\ \frac{5 \times 10^{-4} \left(\frac{\Delta x}{\lambda_D(t)}\right)^3}{M_{\text{ppc}} \left[1 + \left(\frac{r_{\text{sm}}}{\Delta x}\right)^2\right] \left(1 + \frac{r_{\text{sm}}}{\lambda_D(t)}\right)} & \text{for } \frac{1+r_{\text{sm}}/\Delta x}{\sqrt{2}} \lesssim \omega_p t \end{cases} \quad (18)$$

where we use the Dirac delta function $\delta(\omega_p t)$ to reflect the rapid equilibration of electric field energy with plasma on short time scales that we have not tried to measure. In the third stage, noise-driven heating, dK_{th}/dt is constant (as long as $\Delta K \ll K_{\text{th}}$); thus K_{th} grows linearly in time, consistent with diffusion in velocity. In all three stages, $\Delta K \propto M_{\text{ppc}}^{-1}$; thus particle weight can play an important role in unphysical energy exchanges (see, e.g., [Lawson & Gray, 1991](#); [Jubin et al., 2024](#)).

Figure 7 shows the accuracy of this empirical formula for 11 simulations covering a range of v_B , initial v_{th} [i.e., $\lambda_D(0)$], M_{ppc} , r_{sm} , and Δt . Each pair of lines, connected by thin vertical segments, shows the evolution of $\Delta K(t)$ —the line with symbols is simulation data, and the line without symbols is a numerical time-integration of Eq. (18). The fit is good within a factor of a few, except for some small shifts in time.

In the first stage, $\omega_p t \lesssim 0.5$, some plasma energy is immediately lost to the electric field as the initial state with perfectly-correlated particle positions and $E = 0$ gives way to a less-correlated (but far from uncorrelated) state with $E \sim E_{\text{rms}}$ (cf. [Acciarri et al., 2024a,b](#)). Accordingly, $\Delta K < 0$ at the earliest times shown in Fig. 7; smoothing reduces this effect. However, with smoothing ($r_{\text{sm}} \gtrsim \Delta x$) there is a second stage where the plasma continues to lose energy linearly in time ($\Delta K \propto -t$, paralleling the solid blue lines) over a longer period t_{decl} , until it has lost a fraction $\sim 0.3/M_{\text{ppc}}$ of its original thermal energy. After that (the third stage), ΔK starts growing linearly in time ($\Delta K \propto t$, parallel the ascending solid blue lines), consistent with typical particle velocities diffusing as the square root of time. When ΔK becomes comparable to K_{th} , the diffusive heating slows as $\lambda_D(t)$ becomes better resolved.

With velocity diffusion, and without smoothing ($r_{\text{sm}} = 0$), the energy of one physical electron within a macroparticle grows (during the third stage) on average as

$$\Delta K_1(t) \sim 2.5 \times 10^{-4} (\Delta x/\lambda_D)^3 M_{\text{ppc}}^{-1} m v_{\text{th}}^2 \omega_p t. \quad (19)$$

It is interesting to compare the energy growth with a simplistic random walk in velocity, where particle velocities receive a random kick $\Delta v = \pm e E_{\text{diff}} \tau / m$ (kicks with + and - have equal prob-

Smoothing away grid instability and noise in PIC

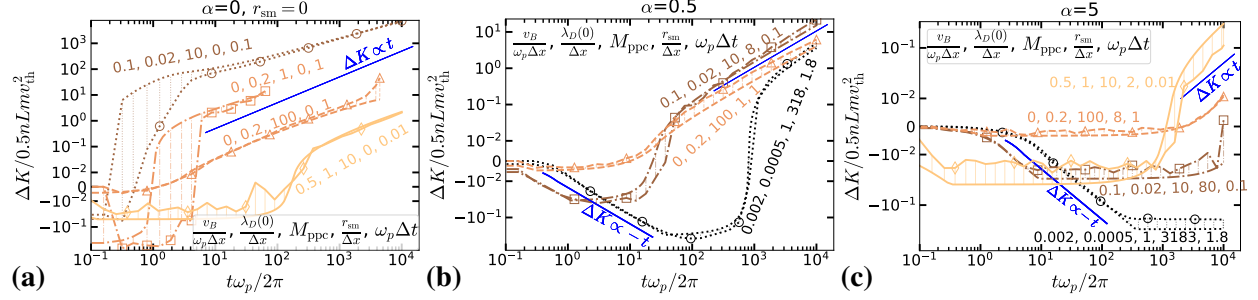


FIG. 7. Each pair of lines, connected by vertical segments, shows the measurement and fit of (unphysical) net change in plasma energy, ΔK , versus time for MC-PIC simulations of uniform plasma. For each pair, the line with symbols shows simulation data and the line without symbols shows numerical integration of Eq. (18). Color indicates the value of $\lambda_D/\Delta x$ at $t=0$, from dark [$\lambda_D(0)/\Delta x = 0.0005$] to light [$\lambda_D(0)/\Delta x = 1$]. For reference, solid blue lines show $\Delta K \propto \pm t$. Aside from small time-shifts, the data and fit are close for a wide range of simulation parameters (see below). In each case, we see the immediate loss in plasma energy ($\Delta K < 0$ at $\omega_p t \ll 1$; stage 1); for $r_{sm} > \Delta x$, energy loss continues as $\Delta K \propto -t$ for time t_{decl} (stage 2). Then (stage 3) the plasma energy starts increasing as $\Delta K \propto t$, consistent with diffusion in velocity. The three panels show simulations with different smoothing, $\alpha = 0, 0.5$, and 5 , from (a) to (c), and in each panel, simulations are labeled individually by $v_B/\omega_p\Delta x$, $\lambda_D(0)/\Delta x$, M_{ppc} , $r_{sm}/\Delta x$, and $\omega_p\Delta t$. The simulations shown here include $v_B/\omega_p\Delta x \in \{0, 0.002, 0.1\}$, $\lambda_D(0)/\Delta x \in \{0.0005, 0.02, 0.2, 1\}$, $M_{ppc} \in \{1, 10, 100\}$, $0 \leq r_{sm}/\Delta x < 3200$, and $0.01 \leq \omega_p\Delta t \leq 1.8$. Simulations that end before $T = 2\pi 10^4/\omega_p$ were halted because more than 1/4 of the particles gained enough energy to cross Δx in time Δt , which usually precedes a rapid energy rise [briefly visible, e.g., for $t\omega_p/2\pi \gtrsim 3000$ in panel (a) ($\alpha = 0$) orange/dashed case with $v_B/\omega_p\Delta x = 0$, $\lambda_D(0)/\Delta x = 0.2$, $M_{ppc} = 100$].

ability) during each interval of time τ . In this model (which depends on choice of E_{diff} and τ),

$$\frac{m}{2} \langle v(t)^2 \rangle \sim \frac{m}{2} \frac{e^2 E_{diff}^2 \tau^2 t}{m^2 \tau} \quad (20)$$

(where angle brackets are ensemble averages), and so comparison with Eq. (19) yields

$$E_{diff} \sqrt{\omega_p \tau} \sim \sqrt{5 \times 10^{-4}} \left(\frac{\Delta x}{\lambda_D} \right)^{3/2} \frac{m v_{th}^2}{e \lambda_D} M_{ppc}^{-1/2} \quad (21)$$

If we speculate that $\omega_p \tau \sim 1$ (which, we will see in the next subsection, works for test particles), then $E_{diff} \sim 0.03 (\Delta x/\lambda_D)^{3/2} \sqrt{1 + \lambda_D/\Delta x} E_{rms}$. For $\lambda_D/\Delta x \gtrsim 0.1$, $E_{diff} < E_{rms}$, so velocity diffusion (especially at $\lambda_D/\Delta x \gg 0.1$) is slower than would be expected from random E_{rms} -sized kicks in every time interval $\sim \omega_p^{-1}$. It is reasonable to suppose that the effective τ depends on $\lambda_D/\Delta x$, but we find this does not satisfactorily explain the entire $\lambda_D/\Delta x$ dependence. Rather, we suspect that the correlations between particle positions prevent particles from experiencing uncorrelated (over τ) fields of magnitude E_{rms} in the way that a test particle would.

Thus we have shown that unphysical energy growth in MC-PIC is consistent with stochastic velocity diffusion, insofar as the energy grows linearly in time. However, we have not produced a model that predicts E_{diff} and τ independently, although we have empirically determined (assuming a simple random walk in velocity) the value and scaling of $E_{diff} \sqrt{\tau}$.

Smoothing away grid instability and noise in PIC

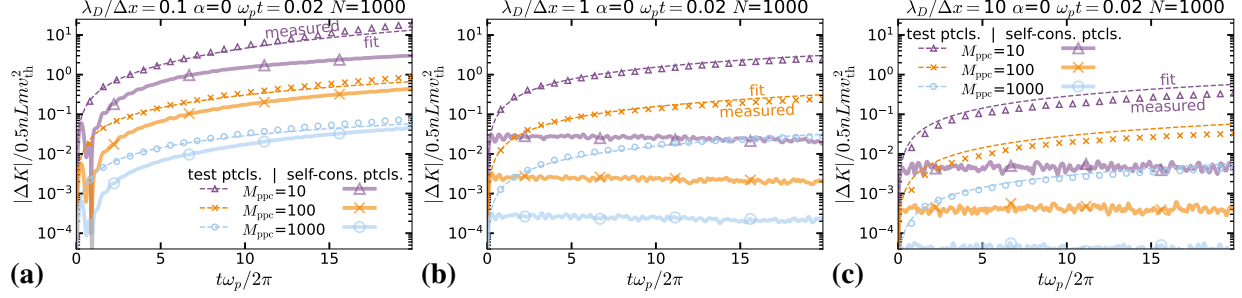


FIG. 8. The change in MC-PIC particle energy over time (normalized to the initial energy) of self-consistent particles (thick, solid lines marked with occasional large symbols) compared with test particles, over the first 20 plasma periods for (from left to right) $\lambda_D/\Delta x = 0.1, 1,$ and 10 . For test particles, (relatively numerous) small symbols show measurements, while thin, dashed lines show a simple fit using Eq. (20) with $E_{\text{diff}} = E_{\text{rms}}$ from Eq. (16) and $\tau = \omega_p^{-1}$. All simulations have $v_B = 0$, $\omega_p \Delta t = 0.02$, and no smoothing. In each case, we show simulations with $M_{\text{ppc}} = 10, 100,$ and 1000 (in purple, orange, and light blue).

G. Test particles do not always mimic MC-PIC particles

In the previous subsection, we suggested that PIC particles exhibit stochastic velocity diffusion, but it is inconsistent with experiencing a different random field of order E_{rms} every time interval $\tau \sim \omega_p^{-1}$. However, test particles—which do not interact—do exhibit this behavior.

Figure 8 shows $|\Delta K(t)|$ for the same simulations as in Fig. 6 (with initially uniform positions and random velocities), but for 20 plasma periods and for both self-consistent particles (thick, solid lines with infrequent, large symbols) and test particles in the same simulation (more numerous, small symbols), for $M_{\text{ppc}} = 10, 100,$ and 1000 . The thin, dashed lines show a simple but surprisingly good fit to the test particles, the result of a random walk given by Eq. (20) with $E_{\text{diff}} = E_{\text{rms}}$ from Eq. (16) and time interval $\tau = \omega_p^{-1}$. The test particles always gain more energy than PIC particles.

For $\lambda_D/\Delta x = 0.1$ the growth in self-consistent particle energy is already significant, and the test particle energy growth is worse, although not much worse in order of magnitude. For $\lambda_D/\Delta x = 1$ and $M_{\text{ppc}} = 10$, the test particles double their energy over 20 plasma periods, compared with less than 2% increase for self-consistent particles; with $M_{\text{ppc}} = 1000$, test particles gain only about 3%, compared with 0.02%. For $\lambda_D/\Delta x = 10$ the use of test particles is more reasonable because E_{rms} is relatively small; however, with $M_{\text{ppc}} = 10$ the test particle energy still grows unphysically by 30% over just 20 plasma periods, compared with a fraction of a percent for self-consistent particles.

Thus it is potentially misleading to use test particles as a proxy for self-consistent particles.

VII. DISCUSSION

We have demonstrated that smoothing the charge density eliminates grid instability in explicit electrostatic MC-PIC simulation, even when $\lambda_D \ll \Delta x$; the key is that, for the smoothing profile given by Eq. (4), the smoothing length r_{sm} must increase as $r_{\text{sm}}/\Delta x \sim \Delta x/\lambda_D$. Perhaps more important, we have shown that statistical particle noise causes diffusion in velocity space, hence thermal energy that grows linearly in time, that worsens for smaller $\lambda_D/\Delta x$, and at least in MC-PIC, this poses a more pressing problem than grid instability. Fortunately, smoothing suppresses noise as well as grid instability. Unfortunately, smoothing degrades the effective spatial resolution

to (of order) the smoothing length r_{sm} . While the preceding presentation focused on stabilizing simulations with a given Δx , we now consider how to choose Δx and r_{sm} optimally, given a fixed resolution requirement. What is the potential computational advantage of this approach?

A good estimate will be specific to the physics applicable to the particular problem being solved. Here, we will assume that the problem is such the smallest important length scale is the scale on which the electric field and particle distribution vary (as opposed to some other physics, such as a mean free path; e.g., some PIC simulations with Monte Carlo collisions might have their resolution determined by a mean free path, even though the electric field and particle distribution vary on much larger scales, and smoothing might not degrade the resolution for collisions at all, leading to very different considerations). We will write this smallest scale to be resolved as $\Delta x_{\text{ideal}} \equiv \eta \lambda_D$, where $\eta > 1$.

Under these conditions, the optimal simulation (with largest cell size) will have $r_{\text{sm}} \sim \eta \lambda_D$ (since r_{sm} is the effective resolution), hence $\Delta x \sim \eta^{1/2} \lambda_D$ (since $r_{\text{sm}}/\Delta x \sim \Delta x/\lambda_D$). I.e., the optimal cell size is the geometric mean of λ_D and the required spatial resolution.

Compared with an unsmoothed (standard) simulation with cell size $\Delta x_s \sim \lambda_D$, the increase in cell size $\Delta x/\Delta x_s \sim \eta^{1/2}$ can potentially speed up the field solve, presumably by at least a factor $\eta^{1/2}$, but possibly $\eta^{p/2}$ for some power $p \geq 1$ that depends on the field solve algorithm (and on the dimensionality, when we consider 2D and 3D). However, the smoothing operation is essentially a second field solve, yielding a net gain of $\eta^{p/2}/2$, if we ignore particle-related costs.

However, many PIC simulations are dominated by particle-related costs. In such cases, reducing the field solve time does not speed up overall computation. Any gains require a reduction in the total number of particles. Since smaller $\lambda_D/\Delta x$ exacerbates noise, requiring more particles per cell, suppressing noise is crucial. With smoothing, M_{ppc} may be kept constant (at a small number, perhaps as small as 1 or 10) as Δx is increased. In that case, computation would speed up by a factor $\eta^{1/2}$ (and possibly by $\eta^{d/2}$ in d dimensions, although PIC noise may scale differently in 2D and 3D, so this requires future study).

In addition, if the simulation does not need to resolve the plasma frequency well, the time step can be increased from roughly $\Delta t \sim \Delta x/3v_{\text{th}} \sim \lambda_D/3v_{\text{th}} = 1/3\omega_p$ (required to keep most particles from traveling more than Δx in time step Δt , when $\Delta x \sim \lambda_D$) to $\Delta t \sim 2/\omega_p$ (for $\Delta x \gg \lambda_D$, the Courant-Friedrichs-Lewy time step is the limitation, not the maximum distance traveled). Thus, in such cases, larger cells and smoothing allow the time step to be increased by ~ 6 .

A hypothetical ideal PIC algorithm might allow larger cell size $\Delta x \sim \eta \lambda_D$. Although past attempts to find such algorithms have focused on defeating grid instability, we argue that particle noise is an equally urgent problem, if not more urgent. Equation (18) characterizes how noise-driven heating depends on numerical parameters Δx , M_{ppc} , and r_{sm} . Although practical simulations with non-uniform plasma may have other considerations, this result for uniform plasma provides a good starting point to determine optimal parameters for a given noise tolerance. For standard unsmoothed PIC ($r_{\text{sm}} = 0$), the rate of noise-driven heating, dK_{th}/dt , scales as $(\Delta x/\lambda_D)^3 M_{\text{ppc}}^{-1}$. If the scaling of the PIC algorithm is known with respect to Δx and M_{ppc} , we can find their optimal values for the maximum tolerable dK_{th}/dt . We suspect that most simulations will be optimized by using smaller $\Delta x \sim \lambda_D$ rather than suffer the higher M_{ppc} required to reduce noise when $\Delta x \gg \lambda_D$, even if grid instability were not a consideration. The introduction of smoothing ($r_{\text{sm}} > \Delta x$) can keep noise tolerable with larger Δx and lower M_{ppc} (as we demonstrated in the previous section), since dK_{th}/dt scales as $(\Delta x/\lambda_D)^3 [M_{\text{ppc}}(1 + (r_{\text{sm}}/\Delta x)^2)(1 + r_{\text{sm}}/\lambda_D)]^{-1}$. Ultimately, the optimal parameters will depend on the PIC algorithm scaling, but it is likely that smoothing can significantly reduce computational costs when under-resolving the Debye length.

A different smoothing kernel might yield a more efficient relationship between resolution and

stability. We leave such exploration to future work, but we reiterate that the relationship $r_{\text{sm}}/\Delta x \sim \Delta x/\lambda_D$ was derived to stabilize the shortest (Nyquist) wavenumber specifically for a smoothing kernel with Fourier transform $(1 + k^2 r_{\text{sm}}^2)^{-1} \sim (k r_{\text{sm}})^{-2}$. In analogy with the derivation of Eq. (5), a smoothing kernel that, at $k r_{\text{sm}} \gg 1$, scales as $(k r_{\text{sm}})^{-p}$ (for some $p > 0$), will stabilize the Nyquist wavenumber for $r_{\text{sm}}/\Delta x \sim (\Delta x/\lambda_D)^{2/p}$. Higher values of p thus stabilize the shortest wavelengths with smaller r_{sm} , but stabilizing longer wavelengths might require larger r_{sm} .

VIII. SUMMARY

This paper focuses on three aspects of enabling electrostatic PIC simulation with under-resolved Debye length: smoothing to defeat grid instability, smoothing to defeat particle noise, and an efficient, flexible smoothing algorithm:

1. By writing down the MC-PIC dispersion $D(\omega, k)$ with spatial discretization, we showed that for any fixed k , smoothing the charge density on the grid changes the dispersion in the same way as decreasing the plasma density (hence increasing its Debye length λ_D). Knowing the change in density (or in λ_D) that would yield stability, we can calculate the smoothing that yields stability (for a given k). This applies to any PIC algorithm with a dispersion of similar general form.
 - With the rough form of $D(\omega, k)$ and empirical knowledge of the minimum stable density (i.e., such that $\lambda_D \gtrsim \Delta x$), we determined the amount of smoothing needed to stabilize the shortest-wavelength modes. [§III]
 - We find that smoothing with Eq. (4) eliminates grid instability when the smoothing radius r_{sm} scales as $r_{\text{sm}}/\Delta x = (\alpha/\pi)\lambda_D/\Delta x$, where α is a constant of order unity. [§V]
 - Other smoothing profiles could potentially yield stability with smaller r_{sm} . [§III]
 - Without smoothing, the most unstable mode usually has $k \sim \pi/\Delta x$. Smoothing decreases the fastest-growing mode k . [§V]
 - By exhaustively finding the roots of $D(k, \omega)$ for a Cauchy-squared distribution, for many k , temperatures, and drift velocities, we found that, for the smoothing given by Eq. (4), the amount of smoothing necessary for MC-PIC stability is $\alpha \approx 5$ (although $\alpha \approx 2$ might suppress growth enough for some applications). [§V]
 - We did not detect grid instability in MC-PIC simulations (with Maxwellian distributions) with smoothing with $\alpha \geq 0.2$. However, noise-driven heating was so strong for $\alpha \leq 1$ that grid instability might have been present while undetected. [§VIC]
2. We demonstrated how MC-PIC particle noise becomes increasingly disruptive as $\lambda_D/\Delta x$ decreases; for simulations with $\lambda_D < \Delta x$, noise may be an equally or even more important consideration than grid instability.
 - Noise-driven heating grows linearly in time, whereas grid-instability heating grows exponentially [§VIB].
 - Noise-driven heating rates are proportional to M_{ppc}^{-1} , whereas grid instability growth rates become independent of M_{ppc} at large M_{ppc} . [§VIB]
 - E.g., for $\Delta x \approx 5\lambda_D$, grid instability is undetectable even with $M_{\text{ppc}} = 1000$, while noise-driven heating is ruinous. [§V, §VI]
 - For $\Delta x \gtrsim \lambda_D$, it is likely more computationally efficient to reduce noise by reducing Δx (keeping the total number of particles fixed) than by increasing M_{ppc} . [§VIF]
 - The amount of smoothing necessary to eliminate grid instability is roughly the same as the amount needed to suppress noise-driven heating in MC-PIC for small M_{ppc} . [§V, §VIC]
 - The PIC “noise electric field” on the cell scale in 1D, due to *uncorrelated* random particle positions is given by $E_{f\Delta x}$ in Eq. (1) with $f = M_{\text{ppc}}^{-1}$. The energy density of this field is

$\epsilon_0 E_{f\Delta x}^2/2 \sim M_{\text{ppc}}^{-1} n m v_{\text{th}}^2 (\Delta x/\lambda_D)^2/2$. For $\Delta x \gg \lambda_D$, this unphysical field energy can easily exceed the plasma energy. This may be a general concern for any PIC simulation in which particles obtain positions due to mechanisms other than the fundamental PIC algorithm (e.g., initial loading, injection from boundaries, collisions, combining macroparticles). [[§II](#), [§VIE](#)]

- However, the self-consistent electric field has smaller fluctuations than $E_{f\Delta x}$ because particle positions are correlated even on sub-grid scales. We find empirically in MC-PIC that the root mean square field in uniform plasma is

$$E_{\text{rms}} \sim \frac{m v_{\text{th}}^2}{e \lambda_D} \sqrt{\frac{1}{(1 + \lambda_D/\Delta x)(1 + r_{\text{sm}}/\Delta x)}} M_{\text{ppc}}^{-1/2} \quad (22)$$

where r_{sm} is the radius of smoothing used. This agrees roughly with analytical calculations of [Touati et al. \(2022\)](#), and adds the correction for $r_{\text{sm}} > 0$. [[§VID](#)]

- Initialization with random particle positions is disastrous for $\lambda_D \lesssim \Delta x$, unless M_{ppc} is much higher than typically used in PIC. [[§II](#), [§VIE](#)]
- A 1D MC-PIC simulation of uniform plasma (initialized with uniformly-spaced particles with random velocities) exhibits three stages of energy change (or two stages, without smoothing). [[§VIF](#)]

(1) Almost immediately, the electric field grows to E_{rms} at the expense of plasma thermal energy, roughly conserving energy overall. The expression for E_{rms} shows that for $\lambda_D \lesssim \Delta x$ and $r_{\text{sm}} = 0$, this is a relaxation to numerical equipartition (i.e., between electric field and macroparticle degrees of freedom); smoothing reduces this unphysical energy exchange.

(2) With smoothing, $r_{\text{sm}} \gtrsim \Delta x$, the plasma thermal energy continues to decline by a fraction $\sim 0.3/M_{\text{ppc}}$ from its initial value over a time $t_{\text{decl}} \sim (1 + r_{\text{sm}}/\Delta x)/(\sqrt{2}\omega_p)$. The electric field energy does not increase correspondingly, violating energy conservation. The total decline is independent of r_{sm} , although smoothing helps by increasing t_{decl} .

(3) The plasma energy grows linearly in time due to stochastic velocity diffusion (noise-driven heating). The electric field energy grows correspondingly, violating energy conservation.

- We find that, in 1D MC-PIC, these three stages of changing thermal energy K_{th} can be described quantitatively by:

$$\frac{1}{\omega_p K_{\text{th}}(t)} \frac{dK_{\text{th}}}{dt}(t) \sim \begin{cases} -\frac{\delta(\omega_p t)}{2M_{\text{ppc}}(1 + \lambda_D/\Delta x)(1 + r_{\text{sm}}/\Delta x)} & \text{for } \omega_p t \approx 0 \\ -\frac{0.3\sqrt{2}}{M_{\text{ppc}}(1 + r_{\text{sm}}/\Delta x)} & \text{for } 0 \lesssim \omega_p t \lesssim \frac{1 + r_{\text{sm}}/\Delta x}{\sqrt{2}} \\ \frac{5 \times 10^{-4} \left(\frac{\Delta x}{\lambda_D(t)}\right)^3}{M_{\text{ppc}} \left[1 + \left(\frac{r_{\text{sm}}}{\Delta x}\right)^2\right] \left(1 + \frac{r_{\text{sm}}}{\lambda_D(t)}\right)} & \text{for } \frac{1 + r_{\text{sm}}/\Delta x}{\sqrt{2}} \lesssim \omega_p t \end{cases} \quad (23)$$

Noise-driven heating (the bottom line) increases strongly as $\lambda_D/\Delta x$ decreases below 1. [[§VIF](#)]

- Test particles experience greater velocity diffusion than self-consistent particles. In MC-PIC, test particles diffuse as if receiving a random kick of strength E_{rms} every time interval $\tau = \omega_p^{-1}$. Using test particles (rather than tracking a sample of self-consistent PIC particles) may yield misleading results. [[§VIG](#)]

3. Severely under-resolving the Debye length requires smoothing over many cells; finding a performant smoothing algorithm may be nontrivial. We proposed and tested a smoothing algorithm involving a modified Poisson solve, which is very similar to the Poisson solve used to find the electric potential, except more diagonally dominant. With this approach, we hope the penalty for smoothing will be less than the time required for the already-existing Poisson solve for the potential.
 - The modified Poisson-smoothing offers similar flexibility as the potential solve. For example, if a PIC code has a Poisson solver that can handle variable cell sizes, it can likely be easily modified to perform the smoothing operation for the same conditions. [§IV]

To confirm the effectiveness of smoothing, we showed stable MC-PIC simulation (of a uniform, drifting 1D plasma) with tiny $\lambda_D/\Delta x = 1/2000$ while using just 1 macroparticle per cell, for 10^4 plasma periods (cf. §VIC).

Smoothing degrades the effective spatial resolution of the electric field. For the smoothing described in §IV, the optimal cell size (to achieve an effective electric field resolution of r_{sm}) is $\Delta x \sim \sqrt{\lambda_D r_{\text{sm}}}$ (cf. §VII).

Although we demonstrated this method in standard 1D electrostatic, explicit momentum-conserving PIC for regular Cartesian mesh and periodic boundary conditions, we expect all the elements (including smoothing via modified Poisson solve) to generalize to 2D and 3D, other PIC variants, non-Cartesian and possibly irregular meshes, with embedded metal boundaries. In particular the smoothing via Poisson solve allows spatially-varying r_{sm} , which could be used with variable meshes to resolve sheaths near boundaries or regions of locally dense plasma, while under-resolving the Debye length in the bulk plasma.

Smoothing the current density might well suppress grid instability and noise in electromagnetic PIC algorithms. However, explicit electromagnetic codes likely have a field advance significantly faster than the modified Poisson solve needed for smoothing, so smoothing may be relatively more expensive than in electrostatic PIC.

Although we demonstrated the effectiveness of smoothing with a particular smoothing operation, other smoothing methods and profiles might work as well or better. Developing optimal smoothing methods—in terms of speed and performing the minimum necessary smoothing—could potentially provide important benefits.

Since we considered only explicit PIC algorithms, we did not explore potential gains from increasing the time step beyond $2/\omega_p$. An efficient algorithm that allows this might be combined with smoothing to great advantage (for applications that do not need to resolve the plasma frequency, i.e., in which even long-wavelength Langmuir modes are unimportant). Moreover, because such implicit algorithms typically decrease the simulation plasma frequency below $2/\Delta t$, its imaginary component may be similarly decreased, slowing the grid instability (Brackbill & Forslund, 1982). However, such simulations might still require substantial smoothing to reduce particle noise.

The potentially worst problem we observed with the proposed method for under-resolving the Debye length was the slow unphysical decline of initial plasma thermal energy by a fraction $\sim 0.3/M_{\text{ppc}}$, unaffected by smoothing. That may limit feasibility for simulations with $\Delta x \gg \lambda_D$ if it means that they require $M_{\text{ppc}} \gg 1$. While $M_{\text{ppc}} \gg 1$ is reasonable for PIC simulations where Δx is set to the desired resolution (i.e., the scale on which the plasma varies significantly), it may be an onerous requirement when Δx has to be much smaller than the effective resolution, r_{sm} . The fundamental problem here is perhaps one of equipartition: the need for smoothing to suppress sub-grid modes results in Δx being smaller than ideal, leaving the electric field with more degrees

of freedom than desirable. Future work may need to address this problem; however, at least this is not a continuing instability.

Besides investigating smoothing in 2D and 3D, further work might also explore whether the smoothing length could be set dynamically based on the local plasma density to ensure stability. An especially promising aspect of this method is that it may allow high resolution to resolve λ_D near boundaries for accuracy in modeling sheaths, while under-resolving λ_D in the bulk plasma.

ACKNOWLEDGMENTS

We would like to thank Thomas G. Jenkins and Daniel Main for many helpful discussions. This work was supported by the National Science Foundation, grants PHY 2206904 and PHY 2206647.

AUTHOR DECLARATIONS

The authors have no conflicts to disclose.

DATA AVAILABILITY

The data that support the findings of this study (including a Python script to run PIC simulations and a Mathematica script to find roots of the dispersion) are openly available in the Zenodo repository at [doi:doi:10.5281/zenodo.14984906](https://doi.org/10.5281/zenodo.14984906).

Appendix A: Deriving the finite difference dispersion

The finite-difference plasma dispersion has been derived previously (Langdon, 1970; Birdsall & Langdon, 2004). We show it here for completeness and consistency of notation (e.g., with MKS units).

We want to find the Landau damping (or inverse Landau growth rates) for the 1D Vlasov-Poisson system in a uniform electron plasma with a uniform immobile ion background:

$$\partial_t f(x, v) = -v \partial_x f(x, v) - a(x) \partial_v f(x, v) \quad (\text{A1})$$

$$a(x) = -\frac{e}{m} E(x) = \frac{e}{m} \partial_x \phi(x) \quad (\text{A2})$$

$$-\partial_x^2 \phi(x) = [\rho_{\text{ion}} + \rho(x)] / \epsilon_0 \quad (\text{A3})$$

where $-e$ and m are the electron charge and mass, $\phi(x)$ the electric potential, and $f(x, v)$ the electron distribution; $a(x)$ is the acceleration of an electron at x due to electric field $E(x)$. The electron charge density is $\rho(x) = -e \int f(x, v) dv$, and $\rho_{\text{ion}} = -L^{-1} \int_0^L \rho(x) dx$ is the uniform ion charge density.

It suffices for this paper (and follows earlier treatments) to discretize the Vlasov-Poisson system in infinite space, but not in time, nor in particles—this will correspond to PIC in the limit of an infinite number of simulated particles with tiny time step.

The simplest discretization is the field solve, which involves only the grid with nodes $x_n = n\Delta x$ for integers n .

Smoothing away grid instability and noise in PIC

We use a standard 3-point finite difference (FD) Poisson stencil to relate the gridded charge density ρ_n and ϕ_n :

$$(-\nabla_{FD}^2\phi)_n \equiv \frac{-\phi_{n+1} + 2\phi_n - \phi_{n-1}}{\Delta x^2} = \frac{\rho_{ion} + \rho_n}{\epsilon_0} \quad (\text{A4})$$

where $\phi_n \equiv \phi(x_n)$ and $\rho_n \equiv \rho(x_n)$. We then solve for the edge-center electric field $E_{n+1/2}^e$, and then the nodal field

$$E_{n+1/2}^e = -(\phi_{n+1} - \phi_n)/\Delta x \quad (\text{A5})$$

$$E_n = (E_{n-1/2}^e + E_{n+1/2}^e)/2. \quad (\text{A6})$$

The trickier aspect of discretization involves depositing a particle's charge to the grid charge density, ρ_n , and interpolating the grid (nodal electric field) E_n to particle positions. To do this, we introduce the shape function $S(x_m; x) = S(x_m - x)$ which describes (1) the fraction of charge of a particle at position x that should be deposited to the grid node x_m , and (2) the weight of the nodal electric field $E_m \equiv E(x_m)$ when interpolating the field to particle position x . In principle these shape functions can be different, but standard momentum-conserving PIC codes use the same shape for both, and using different functions would not affect the following analysis. With this, we have:

$$\rho_n = \frac{1}{\Delta x} (-e) \int dv \int dx f(x, v) S(n\Delta x - x) \quad (\text{A7})$$

$$a(x) = -\frac{e}{m} E(x) = -\frac{e}{m} \sum_n E_n S(n\Delta x - x). \quad (\text{A8})$$

After linearization about a plasma with uniform distribution $f_0(x, v) = n_0 F_0(v)$ (where n_0 is the plasma density), hence zero electric field, the spatially-discretized equations are, treating $f(x, v)$, ϕ_n , E_n , and ρ_n as first-order perturbed quantities:

$$\partial_t f(x, v) + v \partial_x f(x, v) = \frac{en_0}{m} \sum_n E_n S(n\Delta x - x) \partial_v F_0(v) \quad (\text{A9})$$

$$(-\nabla_{FD}^2\phi)_n = \frac{\rho_n}{\epsilon_0} = -\frac{e}{\epsilon_0 \Delta x} \int dv \int dx f(x, v) S(n\Delta x - x) \quad (\text{A10})$$

$$E_{n+1/2}^e = -(\phi_{n+1} - \phi_n)/\Delta x \quad (\text{A11})$$

$$E_n = (E_{n-1/2}^e + E_{n+1/2}^e)/2 \quad (\text{A12})$$

We have not spatially discretized $f(x, v)$ or its advective derivative $v \partial_x f$, because we will evolve $f(x, v)$ via the method of characteristics, represented as the sum of discrete particles; i.e., we will not be evaluating $\partial_x f$ directly.

We Fourier transform in time and space, assuming ‘‘modes’’ $e^{i(kx - \omega t)}$ (which are not eigenmodes, because the grid breaks translational symmetry), using the following conventions for gridded (e.g., E_n) and continuous (e.g., $S(x)$) quantities

$$\tilde{E}_k = \sum_n e^{-ikn\Delta x} E_n \quad E_n = \frac{\Delta x}{2\pi} \int_{-\pi/\Delta x}^{\pi/\Delta x} e^{ikn\Delta x} \tilde{E}_k dk \quad (\text{A13})$$

$$\tilde{S}_q = \frac{1}{\Delta x} \int_{-\infty}^{\infty} e^{-iqx} S(x) dx \quad S(x) = \frac{\Delta x}{2\pi} \int_{-\infty}^{\infty} e^{iqx} \tilde{S}_q dq \quad (\text{A14})$$

Smoothing away grid instability and noise in PIC

where $k \in (-\pi/\Delta x, \pi/\Delta x]$, and q is any real value, which we will often write, uniquely, as $q \equiv k + k_g$ for integer g , where $k_g \equiv 2\pi g/\Delta x$ (hence $e^{ik_g n \Delta x} = 1$). The following transforms of convolutions/products will be useful:

$$\frac{1}{\Delta x} \int e^{-i(k+k_g)x} \sum_n E_n S(n\Delta x - x) dx = \tilde{E}_k \tilde{S}_{-k-k_g} \quad (\text{A15})$$

$$\sum_n e^{-ikn\Delta x} \int S(x_n - x) f(x) dx = \Delta x \sum_g \tilde{f}_{k+k_g} \tilde{S}_{k+k_g} \quad (\text{A16})$$

In Fourier space, the gridded field solve can be described as

$$K(k)^2 \tilde{\phi}_k = \tilde{\rho}_k / \epsilon_0 \quad (\text{A17})$$

$$-i\kappa(k) \tilde{\phi}_k = \tilde{E}_k, \quad (\text{A18})$$

where, in continuous space we would have $K(k)^2 = k^2$ and $\kappa(k) = k$, but with our discretization, $K(k)^2 = (4/\Delta x)^2 \sin^2(k\Delta x/2)$ and $\kappa(k) = \sin(k\Delta x)/\Delta x$.

The linearized Vlasov-Poisson equations become

$$-i[\omega - (k + k_g)v] \tilde{f}_{k+k_g} = \frac{en_0}{m} \tilde{E}_k \tilde{S}_{-k-k_g} \partial_v F_0(v) \quad (\text{A19})$$

$$\begin{aligned} \tilde{E}_k &= -i\kappa(k) \tilde{\phi}_k = -i \frac{\kappa(k)}{\epsilon_0 K(k)^2} \tilde{\rho}_k \quad (\text{A20}) \\ &= i \frac{e}{\epsilon_0} \frac{\kappa(k)}{K(k)^2} \sum_g \tilde{S}_{k+k_g} \int \tilde{f}_{k+k_g}(v) dv \end{aligned}$$

Dividing Eq. (A19) by $-i[\omega - (k + k_g)v]$ and integrating over v , and substituting into Eq. (A20),

$$\int \tilde{f}_{k+k_g} dv = \frac{en_0}{m} \tilde{E}_k \tilde{S}_{-k-k_g} \int \frac{\partial_v F_0}{-i[\omega - (k + k_g)v]} dv \quad (\text{A21})$$

$$\begin{aligned} \tilde{E}_k &= i \frac{e^2 n_0}{\epsilon_0 m} \frac{\kappa(k)}{K(k)^2} \sum_g \tilde{S}_{k+k_g} \tilde{E}_k \tilde{S}_{-k-k_g} \int \frac{\partial_v F_0}{-i[\omega - (k + k_g)v]} dv \\ &= -\omega_p^2 \left[\frac{\kappa(k)}{K(k)^2} \sum_g |\tilde{S}_{k+k_g}|^2 \int \frac{\partial_v F_0}{\omega - (k + k_g)v} dv \right] \tilde{E}_k \quad (\text{A22}) \end{aligned}$$

Thus we write the dispersion (compare to Sec. 8-10 of [Birdsall & Langdon, 2004](#))

$$\begin{aligned} D(\omega, k) &= 1 + \frac{\omega_p^2}{K(k)^2} \kappa(k) \sum_g |\tilde{S}_{k+k_g}|^2 \int \frac{\partial_v F_0}{\omega - (k + k_g)v} dv \\ &= 1 - \frac{\omega_p^2}{K(k)^2} \kappa(k) \sum_g \frac{|\tilde{S}_{k+k_g}|^2}{k + k_g} \int \frac{\partial_v F_0}{v - \omega/(k + k_g)} dv \quad (\text{A23}) \end{aligned}$$

Appendix B: The dispersion integral for the Cauchy-squared distribution

For the Cauchy-squared distribution, Eq. (11), the integral in the dispersion, Eq. (6) or Eq. (A23), can be written

$$\begin{aligned} \int \frac{\partial_v F_0(v) dv}{v - \omega/(k + k_g)} &= \int \frac{F_0(v) dv}{[v - \omega/(k + k_g)]^2} \\ &= \int \frac{(2v_{\text{th}}^3/\pi) F_0(v) dv}{[v_{\text{th}}^2 + (v - v_B)^2]^2 [v - \omega/(k + k_g)]^2} \end{aligned} \quad (\text{B1})$$

This integral should be calculated using the Landau prescription described by many plasma textbooks (e.g., the dispersion can be evaluated just as for a Cauchy distribution described in detail in Ch. 13 of Gurnett & Bhattacharjee, 2017). For $\text{Im}[\omega] > 0$, the Landau prescription uses straightforward contour integration (deviating around any poles). This integral is a rational function of ω , and therefore the result is identical to its analytic continuation to $\text{Im}[\omega] < 0$. Thus we can skip the rest of the Landau prescription, which is just a recipe for finding the analytic continuation, and conclude that for all ω ,

$$\int \frac{\partial_v F_0(v) dv}{v - \omega/(k + k_g)} = (k + k_g)^2 \frac{\omega - (k + k_g)v_B + 3i|k + k_g|v_{\text{th}}}{[\omega - (k + k_g)v_B + i|k + k_g|v_{\text{th}}]^3}. \quad (\text{B2})$$

Appendix C: The exact dispersion for a Cauchy-squared distribution

Before solving the numerical dispersion in the next section, we consider the exact physical dispersion for a Cauchy-squared distribution, Eq. (11), in continuous space. The continuous-space dispersion is given by Eq. (A23), but keeping only the term with $k_g = 0$. Using the integral from Appendix B,

$$D_c(\omega, k) = 1 - \frac{\omega/\omega_p - kv_B/\omega_p + 3i|k|\lambda_D}{[\omega/\omega_p - kv_B/\omega_p + i|k|\lambda_D]^3}. \quad (\text{C1})$$

Solving $D_c = 0$ requires solving a cubic equation; its 3 solutions are ω_0 and ω_{\pm} , shown below with their limits for $k\lambda_D \rightarrow 0$:

$$\frac{\omega_{\pm}}{\omega_p} = \frac{kv_B}{\omega_p} - i|k|\lambda_D + \frac{\pm(b^{1/3} + b^{-1/3}) + i3^{-1/2}(b^{1/3} - b^{-1/3})}{2} \quad (\text{C2})$$

$$\rightarrow \frac{kv_B}{\omega_p} \pm (1 + 3k^2\lambda_D^2/2) - 4i|k|^3\lambda_D^3 \quad (\text{as } k\lambda_D \rightarrow 0)$$

$$\frac{\omega_0}{\omega_p} = \frac{kv_B}{\omega_p} - i|k|\lambda_D - i3^{-1/2}(b^{1/3} - b^{-1/3}) \rightarrow -2i|k|\lambda_D \quad (\text{C3})$$

$$\text{where } b \equiv \sqrt{27k^2\lambda_D^2} + \sqrt{1 + 27k^2\lambda_D^2}$$

The real part of ω_{\pm} yields the Bohm-Gross dispersion, exactly as with a Maxwellian or with any one-humped distribution with the same first and second velocity moments. These Langmuir waves are weakly-damped for $|k|\lambda_D \ll 1$ and strongly-damped for $|k|\lambda_D \gtrsim 1$, qualitatively similar to a

Maxwellian but differing in dependence on $k\lambda_D$ (Gurnett & Bhattacharjee, 2017). In addition, there is a third, purely-decaying mode ω_0 ; we will not be concerned with this harmless mode, keeping in mind that the (initial-value) Landau approach does not yield true eigenmodes, much less all the eigenmodes of a system with an infinite number of degrees of freedom (a topic well beyond the scope of this paper; see, e.g., Van Kampen, 1955; Case, 1959).

Appendix D: Solving the numerical dispersion for a Cauchy-squared distribution

The numerical dispersion, Eq. (6) or Eq. (A23), looks like the exact physical dispersion, Eq. (C1), with more poles corresponding to aliases of k (i.e., $k + k_g$); we can rewrite it as follows

$$\begin{aligned} D &= 1 - a_k \sum_g b_{k+k_g} \frac{x - x_{k+k_g} + 2i|y_{k+k_g}|}{(x - x_{k+k_g})^3} \\ &= 1 - a_k \sum_g b_{k+k_g} \frac{1}{(x - x_{k+k_g})^2} \left[1 + \frac{2i|y_{k+k_g}|}{x - x_{k+k_g}} \right] \end{aligned} \quad (\text{D1})$$

for normalized frequency $x \equiv \omega/\omega_p$, with poles (for all integer g) $x_{k+k_g} \equiv (k+k_g)v_B/\omega_p - i|y_{k+k_g}|$, $y_{k+k_g} \equiv (k+k_g)\lambda_D$, and a_k and b_{k+k_g} are related to the field solve and shape functions. Using a linear shape function (shaped like a tent spanning width $2\Delta x$):

$$S(n\Delta x - x) = \Theta(\Delta x - |x - n\Delta x|) \frac{|x - n\Delta x|}{\Delta x} \quad (\text{D2})$$

$$\tilde{S}_{k+k_g} = \frac{4 \sin^2(k\Delta x/2)}{(k+k_g)^2 \Delta x^2} \quad (\text{D3})$$

(where Θ is the Heaviside step function), we obtain $b_{k+k_g} = [(k+k_g)\Delta x]^{-3}$. For a Fourier solve, with $K^2 = k^2$ and $\kappa = k$, we get $a_k = 16 \sin^4(k\Delta x/2)/(k\Delta x)$; for the standard finite difference field solve we use [see explanation of K and κ after Eq. (6)], $a_k = 4 \sin^2(k\Delta x/2) \sin(k\Delta x)$.

Our strategy to find dispersion roots approximates $D(k, x\omega_p)$ for x within a circle centered at x_c (eventually for many different circles covering the range of interest). Within the circle, we retain some terms of Eq. (D1) exactly—namely terms with poles within and near to the circle. The remaining terms are Taylor-approximated as a polynomial in $(x - x_c)$ that is guaranteed to converge within the circle (because there are no poles of D there). Importantly, we can place a rigorous upper bound on the error of truncating the Taylor series, as well as on the error of truncating the sum over g . We can always increase accuracy, while keeping truncation orders the same, by shrinking the size of the circle (and using more circles to cover the area of interest). By multiplying the approximation (of known accuracy) by all its poles, we obtain a polynomial in x , for which can reliably find all the roots.

In more detail, the dispersion $D(k, \omega)$ in Eq. (D1) is one minus a sum of “pole terms”: i.e., each term contains one pole x_{k+k_g} (of order 3). To find roots of $D(k, \omega)$ reliably within a chosen area of the complex ω plane (or, equivalently, the complex x plane) for one k at a time, we cover that area with a set of circles; in each circle we construct a polynomial in x with zeros that approximate the zeros of $D(k, x\omega_p)$; we then find all the polynomial’s zeros, keeping those that lie in the circle. To approximate D around x_c at the center of a circle (with radius to be determined by the approximation’s accuracy), we keep N_{exact} pole terms exactly as they appear in Eq. (D1), always including $g = 0$, plus the $N_{\text{exact}} - 1$ poles nearest x_c . We find R , the distance from x_c to

the first pole not among the N_{exact} poles. For the rest of the terms, corresponding to poles outside a circle of radius R around x_c , we perform a Taylor expansion in x around x_c . Because the poles of all Taylor-approximated terms lie outside R , the Taylor expansions converge for $|x - x_c| < R$. Within a given radius $r < R$, it is tedious but straightforward to place a reasonable upper bound on the error accrued by truncating the Taylor expansion to order N_{Taylor} ; the error is highest for the $g = \pm 1$ terms, and using that as a conservative estimate for all $|g| > 1$ simplifies the process. The smaller r/R is, the smaller N_{Taylor} can be (for a desired error). We can also determine (for a given r) where we can safely truncate the sum over g in Eq. (D1), i.e., choosing G and keeping terms $|g| < G$ without exceeding the desired error. With a straightforward 1D numerical root solve, we can find the largest r that yields the desired accuracy, given N_{Taylor} and N_{exact} .

With N_{exact} exact terms in the sum in Eq. (D1), and the rest of the terms either neglected ($|g| > G$) or Taylor-approximated by a polynomial of order N_{Taylor} , we can write D as a rational function of x ; multiplying the equation $D = 0$ by the product of $(x - x_{k+k_g})^3$ for the N_{exact} poles, we arrive at a polynomial equation of degree $3N_{\text{exact}} + N_{\text{Taylor}}$. We find all the roots of this polynomial, and then keep only the roots within radius r of x_c . We do this for all the circles (x_c, r) , which cover the entire area of interest, and collect all the roots. Because the circles necessarily overlap, some roots inevitably appear multiple times, with slight differences below the maximum allowed error.

We use Mathematica to do this, and once we form the approximate polynomial (for a given circle), we find its roots using a numerical precision of 256 digits (for comparison, standard double precision has about 16 digits). This has been sufficient to find roots with an absolute error less than 10^{-6} for polynomials of degree up to about 64; we “spend” about 32 degrees on the Taylor expansion, allowing inclusion of about 10 poles exactly.

We will not describe the lengthy, systematic process for finding the covering of circles, but show an example in Fig. 9. The transparent magenta disks (radius r) are the regions $|x - x_c| < r$ in which the Taylor expansions are accurate to a part in 10^6 or better; around each magenta disk is a dotted green circle (radius $R > r$) that contains no more than 11 poles. By including these terms exactly, we thus ensure that the Taylor expansions of the remaining terms converge everywhere in R . The Taylor expansions converge within the dotted green circle (radius R), but are guaranteed to be sufficiently accurate only in the magenta. The poles themselves (blue dots) are located along the edges of a Λ -shaped wedge with vertex at the origin ($\omega = 0$); a big advantage of using the Cauchy-squared distribution is that the pole locations are easily described.

For sufficiently large $|\omega|$, all the pole terms [terms in the sum of Eq. (D1)] are small unless ω is near one of the poles—otherwise the terms cannot sum to one (to make $D = 0$). In the limit of large $|\omega|$, we expect solutions for ω to be ever closer to the poles. While this leads to frequencies with arbitrarily large real parts, these unphysical modes are strongly damped (because $\text{Im}[\omega] \ll 0$ at these poles) and, as far as we know, do not affect simulation.

For a given $k\Delta x$, $v_B/\omega_p\Delta x$, and $\lambda_D/\Delta x$, we searched for all solutions ω within $-10 < \text{Re}[\omega/\omega_p] < 10$, and $-11\pi\lambda_D/\Delta x < \text{Im}[\omega/\omega_p] < 20$. Here the lower imaginary bound ensures that the region includes about 10 poles, or about 5 with $\text{Re}[\omega] > 0$ (the vertical or imaginary spacing between poles is $\Delta\text{Im}[\omega]/\omega_p = 2\pi\lambda_D/\Delta x$). Extending the bounds just yields more solutions that are very close to poles, hence strongly damped; moreover, despite searching over much larger bounds in a number of cases, we never found a mode with growth rate above $\text{Im}[\omega] > \omega_p$. Thus this region includes all the modes of interest—all physical modes (corresponding to $g = 0$) and all unphysical growing modes.

Using Mathematica, one core of a desktop computer calculates a solution in a time ranging from a fraction of a second for large $v_B/\omega_p\Delta x$ to about ten minutes or longer for some cases with small $v_B/\omega_p\Delta x$. The results are shown in §V.

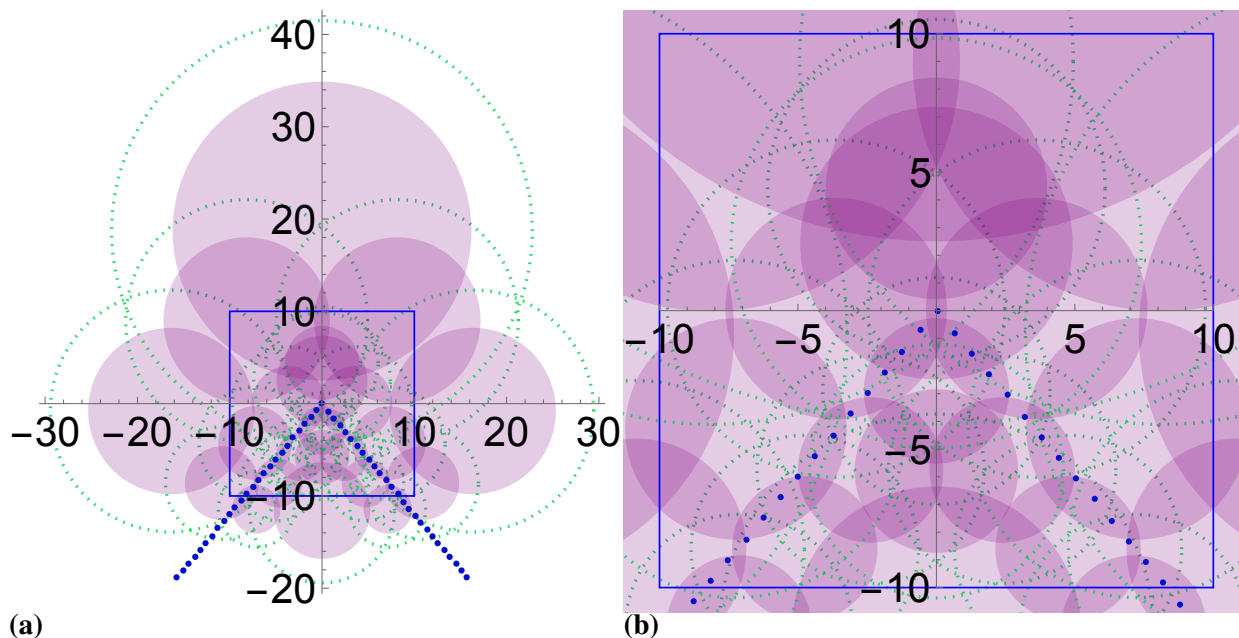


FIG. 9. The 22 circles in the complex ω plane covering region of interest (blue box), $-10 \leq \text{Re}[\omega]/\omega_p \leq 10$ on the horizontal axis and $-10 \leq \text{Im}[\omega]/\omega_p \leq 10$ on the vertical, for $v_B = 0.1\omega_p\Delta x$ and $v_{th} = 0.12\omega_p\Delta x$ (hence $\lambda_D/\Delta x = 0.12$). Panel (b) is the same as (a), but zoomed in. The blue dots show the poles of $D(k, \omega)$. For each magenta disk (of radius r) D was approximated by a different polynomial to find its roots; corresponding to each magenta disk is a dotted green circle showing the radius R containing no more than about 11 poles (the N_{exact} poles).

REFERENCES

- Acciarri MD, Moore C, Beving LP, & Baalrud SD, **2024a**, “When should PIC simulations be applied to atmospheric pressure plasmas? Impact of correlation heating,” *Plasma Sources Sci. Technol.*, 33(3), 035009. DOI:10.1088/1361-6595/ad35e6 arXiv:2403.00656
- Acciarri MD, Moore C, & Baalrud SD, **2024b**, “Artificial correlation heating in PIC simulations,” *Phys. Plasmas*, 31(9), 093903. DOI:10.1063/5.0210881
- Adams LC, Werner GR, & Cary JR, **2025**, “Grid instability growth rates for explicit, electrostatic momentum- and energy-conserving particle-in-cell algorithms,” *in prep.*
- Aguilar X, & Markidis S, **2021**, “A Deep Learning-Based Particle-in-Cell Method for Plasma Simulations,” *arXiv e-prints*, arXiv:2107.02232. DOI:10.48550/arXiv.2107.02232 arXiv:2107.02232
- Barnes DC, & Chacón L, **2021**, “Finite spatial-grid effects in energy-conserving particle-in-cell algorithms,” *Comput. Phys. Commun.*, 258, 107560. DOI:10.1016/j.cpc.2020.107560
- Birdsall CK, & Langdon AB, **2004**, *Plasma physics via computer simulation*, CRC Press
- Birdsall CK, & Maron N, **1980**, “Plasma Self-Heating and Saturation due to Numerical Instabilities,” *J. Comput. Phys.*, 36(1), 1. DOI:10.1016/0021-9991(80)90171-0
- Brackbill JU, & Forslund DW, **1982**, “An Implicit Method for Electromagnetic Plasma Simulation in Two Dimensions,” *J. Comput. Phys.*, 46(2), 271. DOI:10.1016/0021-9991(82)90016-X
- Brackbill JW, & Lapenta G, **1994**, “A Method to Suppress the Finite-Grid Instability in Plasma Simulations,” *J. Comput. Phys.*, 114(1), 77. DOI:10.1006/jcph.1994.1150
- Byers JA, & Grewal M, **1970**, “Perpendicularly Propagating Plasma Cyclotron Instabili-

- ties Simulated with a One-Dimensional Computer Model,” *Phys. Fluids*, 13(7), 1819. DOI:10.1063/1.1693160
- Case KM, **1959**, “Plasma oscillations,” *Annals of Physics*, 7(3), 349. DOI:10.1016/0003-4916(59)90029-6
- Chen G, & Chacón L, **2014**, “An energy- and charge-conserving, nonlinearly implicit, electromagnetic 1D-3V Vlasov-Darwin particle-in-cell algorithm,” *Comput. Phys. Commun.*, 185(10), 2391. DOI:10.1016/j.cpc.2014.05.010 arXiv:1310.1832
- Chen G, Chacón L, & Barnes DC, **2011**, “An energy- and charge-conserving, implicit, electrostatic particle-in-cell algorithm,” *J. Comput. Phys.*, 230(18), 7018–7036. DOI:10.1016/j.jcp.2011.05.031 arXiv:1101.3701
- Chen L, Bruce Langdon A, & Birdsall CK, **1974**, “Reduction of the Grid Effects in Simulation Plasmas,” *J. Comput. Phys.*, 14(2), 200. DOI:10.1016/0021-9991(74)90014-X
- Degond P, Deluzet F, Navoret L, Sun AB, & Vignal MH, **2010**, “Asymptotic-Preserving Particle-In-Cell method for the Vlasov-Poisson system near quasineutrality,” *J. Comput. Phys.*, 229(16), 5630. DOI:10.1016/j.jcp.2010.04.001
- Evstatiev EG, & Shadwick BA, **2013**, “Variational formulation of particle algorithms for kinetic plasma simulations,” *J. Comput. Phys.*, 245, 376. DOI:10.1016/j.jcp.2013.03.006 arXiv:1210.3743
- Fiuza F, Marti M, Fonseca RA, Silva LO, Tonge J, May J, & Mori WB, **2011**, “Efficient modeling of laser-plasma interactions in high energy density scenarios,” *Plasma Phys. Controlled Fusion*, 53(7), 074004. DOI:10.1088/0741-3335/53/7/074004 arXiv:1205.3115
- Gitomer SJ, & Adam JC, **1976**, “Multibeam instability in a Maxwellian simulation plasma,” *Phys. Fluids*, 19(5), 719. DOI:10.1063/1.861518
- Gurnett DA, & Bhattacharjee A, **2017**, *Introduction to Plasma Physics*. <https://ui.adsabs.harvard.edu/abs/2017ipp...book....G>
- Hockney RW, **1971**, “Measurements of Collision and Heating Times in a Two-Dimensional Thermal Computer Plasma,” *J. Comput. Phys.*, 8(1), 19. DOI:10.1016/0021-9991(71)90032-5
- Jubin S, Powis AT, Villafana W, Sydorenko D, Rauf S, Khrabrov AV, Sarwar S, & Kaganovich ID, **2024**, “Numerical thermalization in 2D PIC simulations: Practical estimates for low-temperature plasma simulations,” *Phys. Plasmas*, 31(2), 023902. DOI:10.1063/5.0180421 arXiv:2401.06057
- Langdon AB, **1970**, “Effects of the Spatial Grid in Simulation Plasmas,” *J. Comput. Phys.*, 6(2), 247. DOI:10.1016/0021-9991(70)90024-0
- Langdon AB, **1973**, ““Energy-Conserving” Plasma Simulation Algorithms,” *J. Comput. Phys.*, 12(2), 247–268. DOI:10.1016/S0021-9991(73)80014-2
- Lapenta G, & Markidis S, **2011**, “Particle acceleration and energy conservation in particle in cell simulations,” *Phys. Plasmas*, 18(7), 072101. DOI:10.1063/1.3602216
- Lawson WS, & Gray PC, **1991**, “Heat Flow between Species in One-Dimensional Particle Plasma Simulations,” *J. Comput. Phys.*, 95(1), 195–211. DOI:10.1016/0021-9991(91)90259-N
- Lewis HR, **1970**, “Energy-Conserving Numerical Approximations for Vlasov Plasmas,” *J. Comput. Phys.*, 6(1), 136–141. DOI:10.1016/0021-9991(70)90012-4
- Markidis S, & Lapenta G, **2011**, “The energy conserving particle-in-cell method,” *J. Comput. Phys.*, 230(18), 7037. DOI:10.1016/j.jcp.2011.05.033 arXiv:1108.1959
- Mitchell MS, Miecznikowski MT, Beylkin G, & Parker SE, **2019**, “Efficient Fourier basis particle simulation,” *J. Comput. Phys.*, 396, 837. DOI:10.1016/j.jcp.2019.07.023 arXiv:1808.03742
- Okuda H, **1972a**, “Verification of Theory for Plasma of Finite-Size Particles,” *Phys. Fluids*, 15(7), 1268. DOI:10.1063/1.1694076

- Okuda H, [1972b](#), “Nonphysical Noises and Instabilities in Plasma Simulation due to a Spatial Grid,” *J. Comput. Phys.*, 10(3), 475. [DOI:10.1016/0021-9991\(72\)90048-4](#)
- Powis AT, & Kaganovich ID, [2024](#), “Accuracy of the explicit energy-conserving particle-in-cell method for under-resolved simulations of capacitively coupled plasma discharges,” *Phys. Plasmas*, 31(2), 023901. [DOI:10.1063/5.0174168](#) [arXiv:2308.13092](#)
- Press WH, Teukolsky SA, Vetterling WT, & Plannery BP, [2002](#), *Numerical Recipes in C++: The Art of Scientific Computing*, Cambridge University Press, New York, 2nd ed.
- Reza M, Faraji F, & Knoll A, [2022](#), “Resolving multi-dimensional plasma phenomena in Hall thrusters using the reduced-order particle-in-cell scheme,” *J. Electric Propulsion*, 1(1), 19. [DOI:10.1007/s44205-022-00019-6](#)
- Reza M, Faraji F, & Knoll A, [2023](#), “Concept of the generalized reduced-order particle-in-cell scheme and verification in an axial-azimuthal Hall thruster configuration,” *J. Phys. D Appl. Phys.*, 56(17), 175201. [DOI:10.1088/1361-6463/acbb15](#)
- Shalaby M, Broderick AE, Chang P, Pfrommer C, Lamberts A, & Puchwein E, [2017](#), “SHARP: A Spatially Higher-order, Relativistic Particle-in-cell Code,” *Astrophys. J.*, 841(1), 52. [DOI:10.3847/1538-4357/aa6d13](#) [arXiv:1702.04732](#)
- Touati M, Codur R, Tsung F, Decyk VK, Mori WB, & Silva LO, [2022](#), “Kinetic theory of particle-in-cell simulation plasma and the ensemble averaging technique,” *Plasma Phys. Contr. F.*, 64(11), 115014. [DOI:10.1088/1361-6587/ac9016](#) [arXiv:2208.06375](#)
- Van Kampen NG, [1955](#), “On the theory of stationary waves in plasmas,” *Physica*, 21(6), 949–963. [DOI:10.1016/S0031-8914\(55\)93068-8](#)